

The Physical and Mechanical Properties of an Argillaceous Limestone



Benjamin Hekimi
Department of Civil Engineering and Applied Mechanics
McGill University, Montréal
December 2012

A Thesis submitted to McGill University in partial
fulfillment of the requirements of the degree of
Master of Engineering

© Benjamin Hekimi 2012

Abstract

This thesis presents the work undertaken to characterize the mechanical, physical and fabric characteristics of the argillaceous Lindsay-Cobourg Limestone (LCL), which is a candidate host rock for the construction of a Deep Ground Repository (DGR) for storing low and intermediate level radioactive waste. The work includes a range of tests that were conducted to determine the fabric of the rock, the physical properties of the discrete species of rock and the bulk hydraulic and mechanical properties of representative volume elements of the rock. Emphasis is placed on the application of the “Plug Test” developed at McGill for estimating the tensile strength of the rock as a convenient alternative to the conventional tests such as the Brazilian splitting test. The influence of stratification on the estimation of tensile strength of the LL is discussed.

Résumé

Cette thèse décrit le travail entrepris pour caractériser la roche calcaire argileuse Lindsay-Cobourg (LCL), une strate géologique candidate pour la construction du Deep Ground Repository (DGR), un site pour disposer de déchets radioactifs de niveau d'intensité basse ou moyenne. La recherche inclut des expériences pour déterminer la résistance à la compression et la traction, les propriétés physiques, la perméabilité et la composition du matériau. La recherche porte principalement sur des expériences sur la résistance à la traction, ce qui inclut une méthode alternative pour tester la résistance d'un matériau cassant, le test d'expansion de la cavité centrale, ainsi que la plus traditionnelle méthode indirect dite « Brésilienne ». L'effet de l'anisotropie du LCL est discuté dans le cas des expériences sur la résistance à la traction.

Acknowledgments

I would like to express my thanks to my supervisor, Professor A.P.S. Selvadurai, for defining the scope of the research and for allowing the use of the research material completed in connection with a NSERC Strategic Grant, as well as for all his help and encouragement. The permission to use the “Plug Test” developed by Professor A.P.S. Selvadurai and Dr. R.P. Benson prior to the publication of the results conducted on Stanstead Granite is gratefully acknowledged. I am also grateful to a number of individuals who provided technical support, which enabled the planning and the conduct of the research. Mr. John Bartczak assisted in several aspects on the research. The recovery of the blocks of the LCL from the St. Marys Cement Quarry was planned by Mr. Bartczak and the preparation of the slabs at Pierre Expert was coordinated by Mr. A. Letendre and Mr. L. Jenner. The assistance of the quarry coordinator, Mr. Nick Papanicolaou, in granting access to the St. Marys Cement Quarry in Bowmanville, ON, is also gratefully acknowledged. Mr Paul Selvadurai assisted in the preparation of the samples used for the digital reconstruction. Mr. Antoine Letendre and Mr Luc Jenner conducted many of the permeability tests reported in this thesis. The preparation of samples for strength testing was aided by Mr Gerard Bechard, Mr Mark Selvadurai and Mr Michael Boyd. A special thanks to Sally Selvadurai for her extensive editorial corrections. Finally, I would like to acknowledge Dr. Peter Vilks for reviewing my thesis and providing constructive advice and recommendations.

Support for this research was provided through a Discovery Grant and a NWMO Research Grant awarded to A.P.S. Selvadurai. I also wish to acknowledge the financial support received through the following scholarships, NSERC CGS – M, Bourse de Maitrise en génie Hydro-Quebec.

Table of Contents

Abstract	ii
Résumé.....	ii
Acknowledgments.....	iii
Table of Contents	iv
List of Figures	vi
List of Tables	vii
1. Introduction.....	1
1.1 Objective	1
1.2 Rationale for the Research	3
1.2.1 Compressive Strength	3
1.2.2 Tensile Strength	4
1.2.3 Permeability	4
1.2.4 Physical Properties.....	5
2. The Lindsay-Cobourg Limestone (LCL)	6
2.1 Geology of the Lindsay-Cobourg Formation.....	7
2.2 Chemical and Mineralogical Composition	7
2.3 Saturation of Samples	9
2.4 Digital Representation of the Heterogeneity of LCL.....	9
2.5 Micro-sample Testing of the Permeability of LCL.....	11
2.5.1 Sample Preparation	12
2.5.2 Apparatus	14
2.5.3 Test procedure.....	14
2.5.4 Permeability Results	16
2.6 Physical Properties.....	16
2.6.1 Sample Preparation	17
2.6.2 Methodology	18
2.6.3 Results.....	18
2.7 Physical and Mechanical Properties Summary	19
3. Mechanical strength of Lindsay-Cobourg Limestone.....	22
3.1 Sample Preparation	22
3.1.1 Representative volume.....	22
3.1.2 Sample Preparation – Triaxial and Brazilian Tests.....	24
3.1.3 Sample Preparation – Plug Compression Tests	25
3.2 Compressive Strength	26
3.2.1 The McGill-Hoek cell apparatus.....	26
3.2.2 Methodology	27
3.2.3 p vs q curve	30
3.3 Plug Compression Tests.....	31

3.3.1 Apparatus	31
3.3.2 Methodology	33
3.4 Brazilian Tension Splitting Tests	34
3.4.1 Apparatus	34
3.4.2 Methodology	34
4 Analytical and Computational Modelling.....	36
4.1 Hoop Stress	36
4.1.1 Calculated example	37
4.2 Brazilian test	37
4.3 ABAQUS™ Modelling	39
4.4 Results	41
5. Discussion of Tensile Strength Testing	45
5.1 Variations in results based on methodology	45
5.2 Tensile strength of Lindsay-Cobourg Limestone.....	45
6. Conclusions	47
6.1 Scope for Future Research	48
References	49
Appendices.....	55
Appendix A: Experimental Facilities.....	55
A – 1: Hoek Cell	55
A – 2: GDS Controller Unit	56
A – 3: MTS 315.03 Load Frame	57
A – 4: GDS Tri-axial Cell.....	58
A – 5: Quizix QX-6000HC Dual Piston Pump.....	59
A – 6: Sensotec Model TH EJ load cell	61
A – 7: Blue M drying oven	62
A – 8: Saturation Chamber	63
Appendix B: Photographic Records and the Digitized Images	64
Appendix C: Steady State test data	72
Appendix D: X-ray Diffraction Data	78
Appendix E: X-ray Fluorescence Data	82
F – 1: Canon EOS Camera.....	83
F – 2: Circular saw	84
F – 3: Cleereman drill press	85
F – 4: Coring Equipment.....	86
Appendix G: Software	87
MATLAB™	87
ABAQUS™ FEA.....	87

List of Figures

Figure 1: Cross-Sectional view of the regional geological formation	2
Figure 2: Conceptual model of the Bruce Site stratigraphy	3
Figure 3: The distributions of species in a 406 mm cuboidal block of LCL	6
Figure 4: Crushed samples of dark and light material removed from LCL	8
Figure 5: Converting to black and white images	10
Figure 6: Orthogonal sections in the reconstructed block	11
Figure 7: Thin Disks of Lindsay Cobourg Limestone;	13
Figure 8: Detail of the sample set-up for the LCL permeability steady-state test	15
Figure 9: LCL cores from the DGR borehole	17
Figure 10: Test samples used to obtain the physical properties of LCL	18
Figure 11: Slabs of LCL at various orientations	23
Figure 12: Test specimens	23
Figure 13: Machining the LCL cylinders for conducting the triaxial and splitting tests	24
Figure 14: Preparation procedure of the plug compression tension test specimens	25
Figure 15: The Hoek cell	26
Figure 16: McGill-Hoek cell assembly in the MTS testing facility	28
Figure 17: Schematic of the triaxial compressive strength test setup	29
Figure 18: Typical curve for a triaxial compressive strength test on LCL	29
Figure 19: Progression of stress application during Hoek cell test	30
Figure 20: p vs q curve for Lindsay-Cobourg Limestone	31
Figure 21: Schematic of the central cavity tension test set-up	32
Figure 22: Dismantled plug compression test components	32
Figure 23: Brazilian splitting test apparatus with LCL cylinder	34
Figure 24: Uniform stress applied to the interior cavity of a hollow cylinder	37
Figure 25: Stress distribution during a Brazilian splitting test	38
Figure 26: Physical modeling of the plug compression test	39
Figure 27: ABAQUS™ model for the plug compression test	40
Figure 28: Typical failure patterns of the plug compression test samples	42
Figure 29: Typical load versus displacement curve for the plug compression test	43
Figure 30: Direct tension testing	46

List of Tables

Table 1: Permeability results from steady state flow tests on LCL disks	16
Table 2: Physical Properties of LCL samples from the DGR site	19
Table 3: Summary of Young's modulus estimates for the LCL.....	19
Table 4: Summary of Poisson's ratio estimates for the LCL	20
Table 5: Summary of uniaxial compressive strength estimates for the LCL.....	20
Table 6: Summary of tensile strength estimates for the LCL	20
Table 7: Summary of porosity estimates for the LCL	21
Table 8: Estimates for permeability of LCL reported in the literature	21
Table 9: Results of the plug compression tension tests on LCL.....	41
Table 10: Results of the Brazilian splitting tests on LCL.....	43

1. Introduction

1.1 Objective

The Nuclear Waste Management Organization (NWMO) is the lead agency for developing an adaptive phased management of Canada's nuclear fuel waste (Bill C-27, 2002; NWMO, 2005). In its efforts for developing a site for the disposal of low and intermediate level fuel waste, NWMO has considered several alternatives and has focused in particular on the Lindsay Formation that is located beneath the Bruce Nuclear Reactor site in Tiverton, Ontario, in proximity to Lake Huron. Schematic views of the local stratigraphy and the proposed location of the Deep Ground Repository (DGR) are shown in Figure 1 and Figure 2 respectively (Mazurek, 2004; Gartner Lee Ltd., 2008; Selvadurai et al., 2011). The Lindsay formation is a highly heterogeneous argillaceous limestone which is believed to possess the suitable long term geomechanical properties and so-called self-healing" properties (Thury, 2002; Bastiaens et al., 2007) that allow it to act as a long term isolation medium for the storage of non-heat-emitting low to intermediate level waste. In this research, attention is focused on the characterization of the fabric of the heterogeneous argillaceous rock, its physical and chemical properties and its mechanical properties. This includes failure characteristics and in particular the tensile strength of the rock.

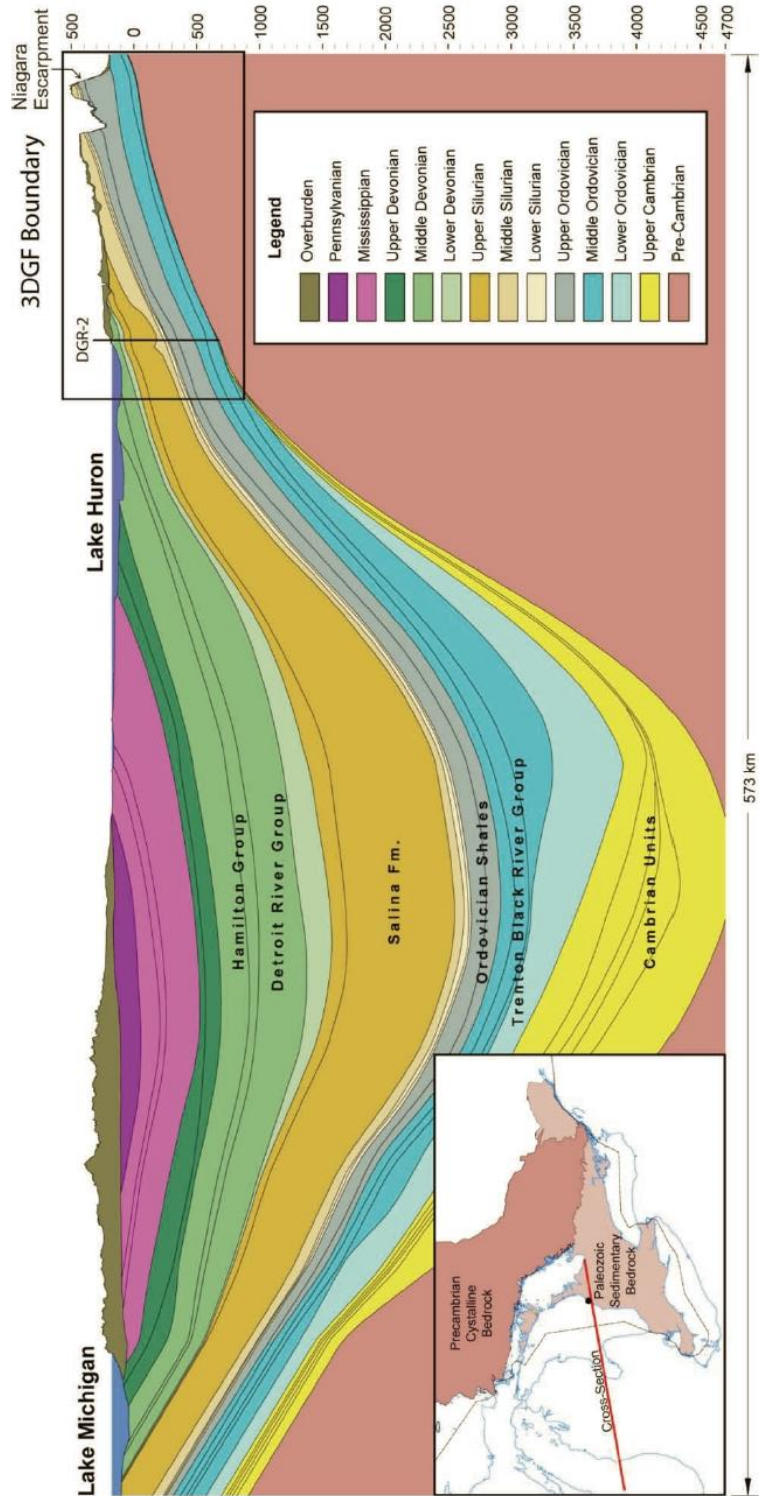


Figure 1: Cross-Sectional view of the regional geological formation (after AECOM Canada Ltd. and Itasca Consulting Canada, Inc., 2011)

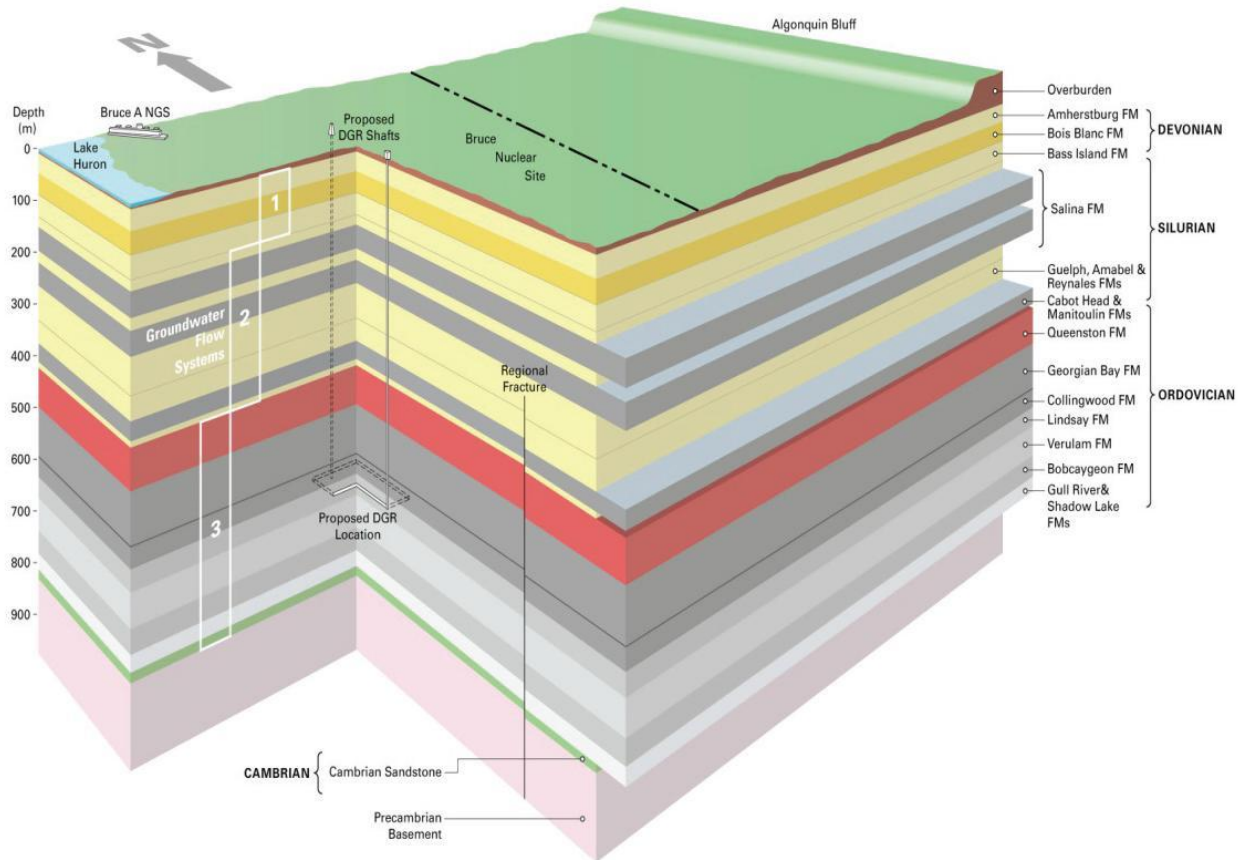


Figure 2: Conceptual model of the Bruce Site stratigraphy (after Gartner Lee Ltd., 2008)

1.2 Rationale for the Research

1.2.1 Compressive Strength

Compressive strength is an important property of brittle materials such as rock or concrete. Components made from these materials often become the principal compressive load bearing elements of a building or facility. Consequently, an accurate and reliable estimate of the compressive strength will result in a safer and less expensive design. In addition, when dealing with an underground facility, it becomes desirable to understand the behaviour of the rock under in situ conditions.

Compressive strength is perhaps the most extensively determined parameter in engineering and effective estimations of the compressive strength of rocks in

particular have been extensively discussed in a number of texts and publications (ISRM, 1978; Bieniawski and Bernede, 1979; Cargill and Shakoor, 1990; Kahraman, 2001; Sonmez et al., 2004; Fener et al., 2005). The work done for this research was conducted using a cell (Hoek type) which was adapted for controlled applications of a triaxial stress state using a pressure controller and a MTS Systems Corporation rock testing machine.

1.2.2 Tensile Strength

A further important engineering property of interest to geomechanical applications is the tensile strength of geomaterials. In openings created underground the initiation of spalling and rock break out will be controlled to a large extent by the tensile strength of the rock. The accurate estimation of the tensile strength of a heterogeneous geomaterial such as the Lindsay Cobourg Limestone is therefore of great interest to the design of the DGR.

It is relatively difficult to determine the tensile strength of brittle materials compared to their compressive strength; for this reason it has been less well researched than compressive strength testing. There are, however, a sizeable number of publications on the various techniques (Mellor and Hawkes, 1971; Broch and Franklin, 1972; Bieniawski and Hawkes, 1978; Okubo and Fukui, 1996; Coviello et al., 2005) used to measure tensile strength in rocks. The most commonly used method is the Brazilian splitting test (ASTM C496 – 11, ASTM D3967 – 08), where the application of a diametral compression at the boundary of a cylinder or disk induces a near uniform tensile stress in the diametral plane. This uniform tensile stress is related to the compressive load applied and serves as a relationship for determining the tensile strength of the material. The studies presented here also utilize the plug compression test for determining the tensile strength of a rock developed at McGill (Selvadurai and Benson, 2013) and applied to estimate the tensile strength of Stanstead Granite.

1.2.3 Permeability

The fluid transport characteristic of a porous medium is a measure of the ability of a fluid to migrate through the connected pore space of the medium. The property

of permeability is an alternative definition of this transport characteristic that takes into account only the properties of the porous medium. The permeability of a porous medium is generally independent of the permeating fluid but can be influenced by environmental factors such as pressure or any reactive processes that can result in dissolution/precipitation of components. Permeability is an important property when considering problems such as natural resources extraction, water resources management (Berkowitz, 2002) and contaminant transport (Bear et al., 1993; Selvadurai, 2006.) In recent years, the permeability of geological media has been of interest in research concerning the disposal of hazardous materials such as nuclear wastes (Chapman and McKinley, 1987; Selvadurai and Nguyen, 1997), geologic sequestration of carbon dioxide (Bachu and Adams, 2003) and geothermal energy extraction (Bataillé et al., 2006).

1.2.4 Physical Properties

Physical properties of a rock relevant to geomechanics applications include its mass density, porosity, water content, thermal conductivity, heat capacity, and coefficient of thermal expansion. The techniques that can be used to measure these properties range from weighing, drying and measuring the volume of the specimen (ISRM 1979) to more complicated experiments such as mercury intrusion porosimetry (Léon Y León, 1998) or x-ray diffraction and fluorescence. These tests are important for the proper characterization of the rock as well as for development and implementation of computational models that can be used in prediction exercises (Selvadurai and Nguyen, 1995; Alonso et al. 2005). In the studies presented here, the water content, porosity and wet and dry densities of the LCL were obtained. The chemical composition tests were performed using x-ray techniques.

2. The Lindsay-Cobourg Limestone (LCL)

The Lindsay-Cobourg Limestone is a light to dark grey mottled rock, with observable heterogeneity (Figure 3.) It is classified as an argillaceous limestone, composed of a fine-grained matrix of carbonate and clay minerals but containing many small shell and plant fossils that range in size from 2 – 8 mm. The limestone minerals form nodules (10 to 50 mm diameter) of a light gray colour, which are interspersed with by thin discontinuous regions of a darker coloration, similar to shale, containing the clay minerals. The classification provided by Golder Associates (2003), Cavé et al. (2009) described LCL as a very fine-grained, thin to medium bedded and largely micritic, with thin beds of bioclastic calcarenite.

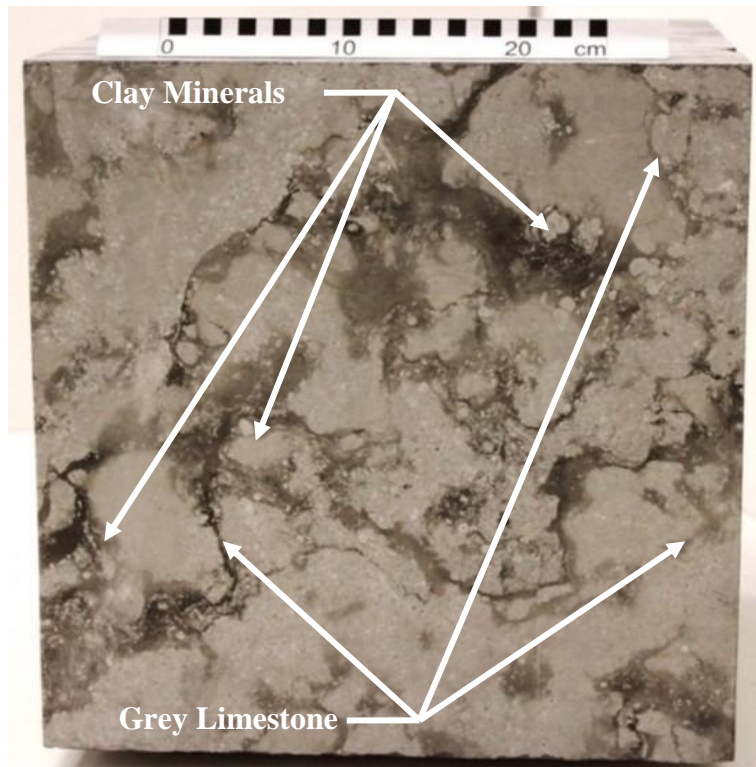


Figure 3: The distributions of species in a 406 mm cuboidal block of LCL

2.1 Geology of the Lindsay-Cobourg Formation

The Lindsay-Cobourg Limestone (LCL) formation is a sub-division of the Middle Ordovician Limestones found in the bedrock in Southern Ontario, within the Michigan Basin. At the proposed DGR site, the basin consists of near-horizontally bedded sedimentary rock deposits extending 860 m in thickness. Bedrock from the Paleozoic era contains dolostones, limestones, shales, sandstones and evaporite minerals (halite, gypsum/anhydrite). These formations date from the upper Cambrian to the upper Devonian (543 - 354 Ma) (Figure 2.) The Lindsay formation is composed of 2 members where the primary Lindsay formation member overlays the Sherman Falls member (Golder Associates 2003). These subsections are 36 m and 9 m thick, respectively. These sub-formations are distinguished by their compositions. The primary Lindsay Formation consists of fine-grained, thin to medium bedded, nodular shaley limestone. The limestone consists of irregular shaped beds and nodules of fine-grained light grey limestone with thin interbeds of argillaceous black shale. The Sherman Falls member formation contains less argillaceous material than the Primary Formation, and consists of medium to thick beds containing smaller nodules than its overlaying neighbour. (Gartner Lee Limited, 2008). The formation has very consistent lateral continuity and an outcrop is accessible at the St Marys Cement quarry in Bowmanville (Golder Associates, 2003).

2.2 Chemical and Mineralogical Composition

The chemical and mineralogical composition of geomaterials can help predict or interpret the results of tests conducted to determine physical and mechanical properties. For example, the presence of montmorillonite clay minerals in a geomaterial indicates the possibility of swelling during contact with water, causing a decrease in the effective porosity and therefore the permeability. Particle or grain size distribution can also affect the porosity and material strength in tension and compression. The LCL has a very fine-grained structure with a very low porosity compared to many other limestones such as Indiana Limestone or Portland Limestone. As shown in Figure 3, the LCL is composed of two

primary materials: a light carbonate layer and a dark argillaceous layer. The lighter material consists principally of calcite with minor quantities of quartz, anhydrite, pyrite, dolomite and apatite. The darker material, is primarily composed of calcite, but contains a sizeable quantity of fine-grained quartz and aluminosilicate clays (Cavé et al., 2009). In order to verify whether there were any significant differences between the chemical compositions of the limestone samples from the Cobourg site, (where the DGR is to be constructed), and the samples extracted from the Bowmanville quarry (used for most of this research), x-ray fluorescence and x-ray diffraction tests were performed on the Bowmanville rock. These tests were conducted on our behalf by the technical staff in the geomechanical laboratories of the Department of Earth and Planetary Sciences at McGill University. The results are presented in Appendices D and E. The material was physically separated into its constituent light and dark components and these were crushed so that they could be tested (Figure 4.) The test results were comparable to those obtained for the Cobourg site by Cavé et al. (2009). There was no significant difference in chemical composition save for the presence of dolomite in the darker material instead of the lighter one.

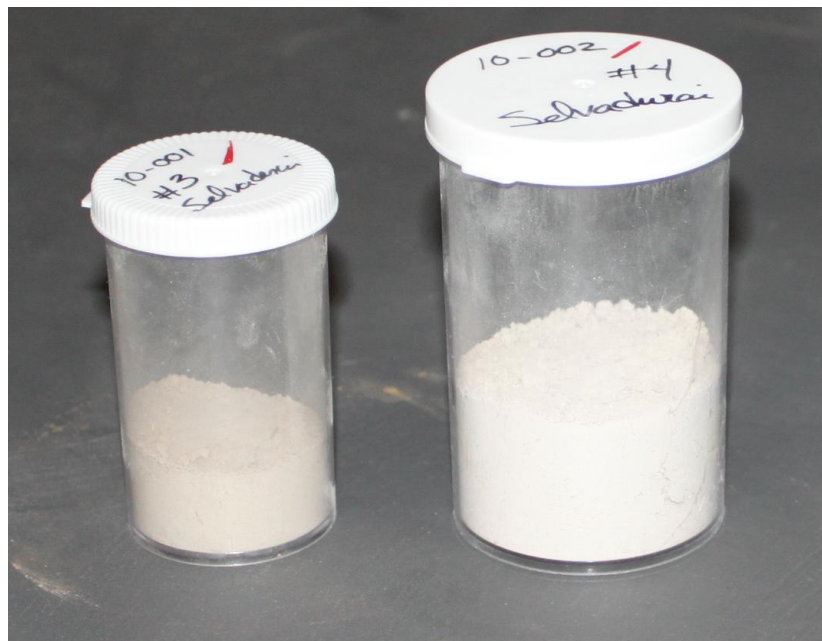


Figure 4: Crushed samples of dark and light material removed from LCL

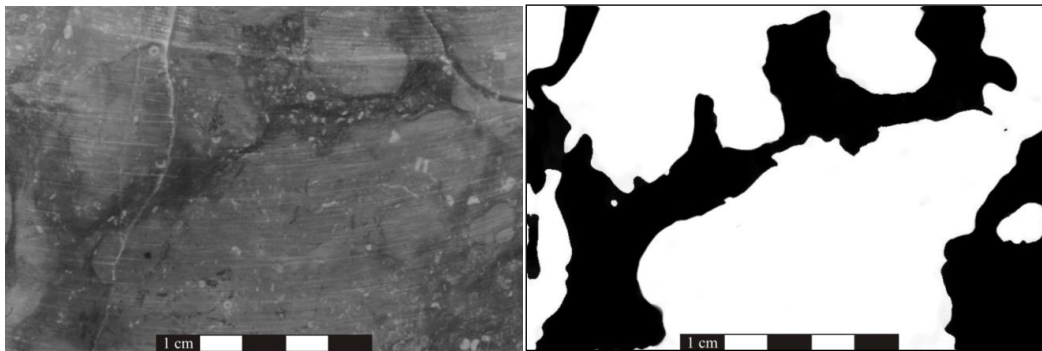
2.3 Saturation of Samples

The degree of saturation of a porous material with a given fluid is a key factor when performing strength or permeability tests; in the case of permeability, correct estimates cannot be obtained unless the connected pore space is fully saturated with the permeating fluid. For example, multi-phase flow or dissolved air in a solution may result in inaccuracies due to surface tension effects (Selvadurai and Glowacki, 2008). There are several methods for saturating porous media: these include submerging samples in water (Dewaele et al., 1991), vacuum saturation (Hearn and Mills, 1991), vacuum saturation combined with sample vibration (Selvadurai and Glowacki, 2008), or forcing fluid through the pore structure until saturation occurs (Banthia and Mindess, 1989). In the case of the permeability tests that will be described below, the LCL specimens were in a saturated state; however, for the strength tests conducted on the LCL, the material was tested in an “as supplied” state, and was not saturated or set to oven dry. This was done because the very low permeability of the LCL requires weeks or even months to achieve complete saturation of the porespace. Consequently, because the specimens were stored in the open air, the rock could only be regarded as being partially saturated.

2.4 Digital Representation of the Heterogeneity of LCL

Geomaterials by their very nature are heterogeneous (Selvadurai 1996, 2004, 2007.) This heterogeneity is a result of a variety of effects associated with deposition, chemical transformations, stress-induced damage and material dissolution. The variability of mechanical and physical properties associated with such heterogeneity can influence the interpretation of parameter identification, particularly if the heterogeneity constitutes a significant part of the specimen being tested (i.e. effects of scale or the choice of a representative volume element (RVE)). In order to obtain a better estimate of the proportions of the two principal geological components encountered in LCL, a photographic method for recreating a 3D model of a sample block was employed. The block used in this investigation measured 80 mm x 120 mm x 300 mm and was obtained from the

St. Mary's Quarry in Bowmanville, Ontario. The block was then cut into samples of dimensions 80 mm x 120 mm x 8 mm using a circular diamond saw blade (Appendix F) with a separation between cuts of approximately 8 mm. Photographs of the thin LCL samples were taken using a tripod in a fixed position. Each thin sample was photographed on both sides. In order to improve the contrast between the two phases of the LCL, the photographs were taken while the surface of the sample was wet. To simulate a unique frame of reference, a mirror image was obtained from the second photographs of each sample. The photographs were then converted into binary images using the *Image Processing Package* provided in MATLAB[®] (Figure 5). The surface of the LCL samples contained a sparse distribution of fossils inclusions and striations left by the diamond saw cut that gave rise to noise in the transformed black and white images. While it was possible to use filtering algorithms to remove this noise, it was more convenient to remove the imperfections manually, using the CorelDRAW[™] X4 Graphics Suite. The complete records for of the photographs and their black and white analogues are presented in Appendix B.



(a) Greyscale image

(b) Black and white

Figure 5: Converting to black and white images

The resulting set of black and white images was then used to construct a 3D model of the cuboidal block of LCL. The data was interpolated using a smoothing function available in MATLAB[™] to create a more realistic profile for the computer generated image of the block. The interpolation process does not seem

to introduce any significant bias towards black or white voxels. From there it is possible to estimate the volume fraction of the block or the area fraction for a particular plane located within it. For this block, the volume fraction for the grey limestone phase is estimated at 0.542. The area fraction of the grey limestone of individual cross sections can vary due to the inhomogeneous nature of the rock. The orthogonal cuts shown in Figure 6 have area fractions of grey limestone estimated at 0.560 (top), 0.484 (left) and 0.531 (right).

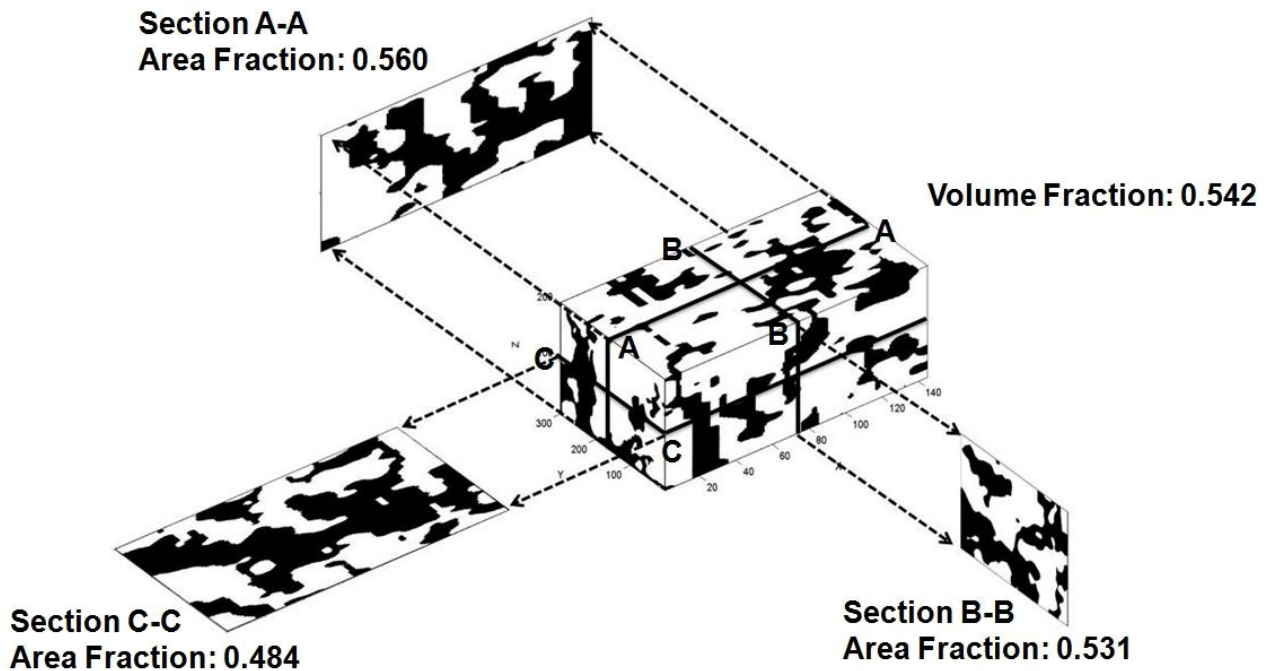


Figure 6: Orthogonal sections in the reconstructed block

2.5 Micro-sample Testing of the Permeability of LCL

The early tests for determining the permeability the LCL were conducted by Intera (1988) on material excavated from the Darlington Generation Station tunnels and the Wesleyville Tunnel exit. A steady state test was used and the permeabilities obtained ranged from 10^{-13} to 10^{-18} m². These values are comparable to those for higher porosity rocks such as Indiana Limestone (Selvadurai and Glowacki, 2008) or Fontainebleau Sandstone (Fredrich et al., 1993), indicating that the tested material may have been damaged in the

excavation process. Additional permeability tests were performed by Raven et al. (1992), Golder Associates (2003), Mazurek (2004) and Gartner Lee Limited (2008) and in these experiments, the permeability measured ranged from 10^{-18} to 10^{-21} m². The most recent results aimed at determining the permeability of LCL were performed at the Environmental Geomechanics Laboratory at McGill University. The results of this research are summarized in the papers by Selvadurai et al. (2011) and Selvadurai and Jenner (2012) and the details are given by Letendre (2010) and Jenner (2011). Selvadurai et al. (2011) tested samples under confining loads using transient tests, and the permeabilities obtained ranged between 10^{-21} and 10^{-23} m². Selvadurai and Jenner (2012) used both transient and steady state testing to determine the radial permeability of unconfined samples; the permeabilities obtained were between 10^{-17} and 10^{-19} m². Most of the limestone tested at McGill University was obtained from the St Marys quarry in Bowmanville, Ontario; however, Selvadurai and Jenner (2012) also tested one specimen obtained from the DRG site.

In order to further investigate the permeability characteristics of LCL, steady state tests were performed on thin (4-5 mm) disks (Figure 7). The objective of the tests was to determine whether the distinct phases of the limestone displayed different permeability characteristics. The hypothesis was that the darker clay material was more permeable than the lighter limestone phase which was most likely an effect of an opened interface between the two phases. The results and observations from the samples tested in Selvadurai and Jenner (2012) seemed to suggest that this might be the case, at least when the samples are unconfined.

2.5.1 Sample Preparation

The test specimens used for these steady state tests differed from the LCL specimens used for the majority of the experiments performed for this research, since they were taken from cores extracted directly from the proposed site of the DGR. This was done in part because the intention was to compare the results obtained from the present experiments with those obtained by Selvadurai et al. (2011) and Selvadurai and Jenner (2012), but also because the material could

actually be cut into disks of 4-5 mm whereas the disks cut from the cores recovered from the St Marys quarry would disaggregate when cut to specimens of small thickness. This discrepancy in the materials, which are believed to be analogous, may be explained by the difference in depth from which the rock was extracted, or by the method by which the quarry material was extracted, namely blasting, resulting in micro-cracks that prevented these thin cuts.



Figure 7: Thin Disks of Lindsay Cobourg Limestone; a) full disk, b) half disk sealed with marine epoxy

To prepare the samples for this research, a core of DGR-LCL was cut using the diamond saw (Appendix F). In order to create a proper sealing surface for the perimeter of the disks during the flow tests, the exterior of the samples was coated with marine epoxy, creating a slightly oversized diameter and a longer sealing length. After an initial test, half the disks' surfaces were coated with epoxy (Figure 7b) in order to test only one of the material phases (i.e. either a larger proportion of the lighter calcite or a larger proportion of the darker argillaceous phase). The digital procedures described in Section 2.4 were used to determine the area and volume fraction of the epoxy treated disk so that subsequent tests on the disks could be used to estimate the permeabilities of the separate phases. The results indicated that there were no significant differences in the measured

permeability of the separate regions so the values are reported simply as a second measurement.

2.5.2 Apparatus

The steady state tests were conducted using a GDS Instruments Inc. triaxial cell apparatus, (Appendix A) This apparatus is designed to test typical rock cylinders with diameters ranging from 25 mm to 100 mm and variable lengths, although it can also be used to conduct permeability tests on the thin disks described previously. The GDS cell was used quite extensively in 35 experiments conducted on Indiana Limestone by Selvadurai and Glowacki (2008) and hydraulic pulse tests on LCL by Selvadurai et al. (2011). A seal was created along the sides of the samples using of a nitrile membrane; because of the extremely low flow rates encountered during this testing, it was important to eliminate any possible leaks. To achieve this, a sealant was used to glue the membrane to the metal platens. In addition, all the compression connections for the tubing were checked to ensure no leakage. In order to diffuse the water along the entire surface of the rock, two thin disks of geotextile fabric were used to sandwich the LCL disk. Figure 8 shows the experimental details and the significant components of the GSD cell.

2.5.3 Test procedure

The triaxial cell is pressurized to a confining pressure of 10 MPa. This pressure was considered to be sufficient to maintain a seal at the interface between the nitrile membrane and the sample. Confining pressures of 5 MPa were used by Selvadurai and Glowacki (2008) to provide sealing between the membrane and the Indiana Limestone cylinder and cell pressures of 10 MPa were used by Selvadurai et al. (2011) during the pulse testing of the LCL. First, a control test was conducted with a stainless steel disk to verify that any leaks in the system were sufficiently below the flow rates used; the test indicated a leakage of an order of magnitude lower than the measured flow rates (i.e. measured flow: 0.0001 – 0.00015 mL/ min, leakage: < 0.00001 mL/min). The pump is then set to supply distilled water at a constant pressure of 2 MPa. During this time, the total flow is monitored and can be used to determine the flow rate and ultimately the

permeability. Despite the thinness of the samples, the flow rate can take in excess of a day to stabilize due to the very low permeability of the LCL. Each sample was tested for a week with three separate runs on the same sample to verify reproducibility; there was a period of zero flow between the tests to allow for the residual pressures to dissipate. Such residual pressures do not generally affect tests conducted at steady state but can influence the results of pulse tests quite significantly (Selvadurai 2009).

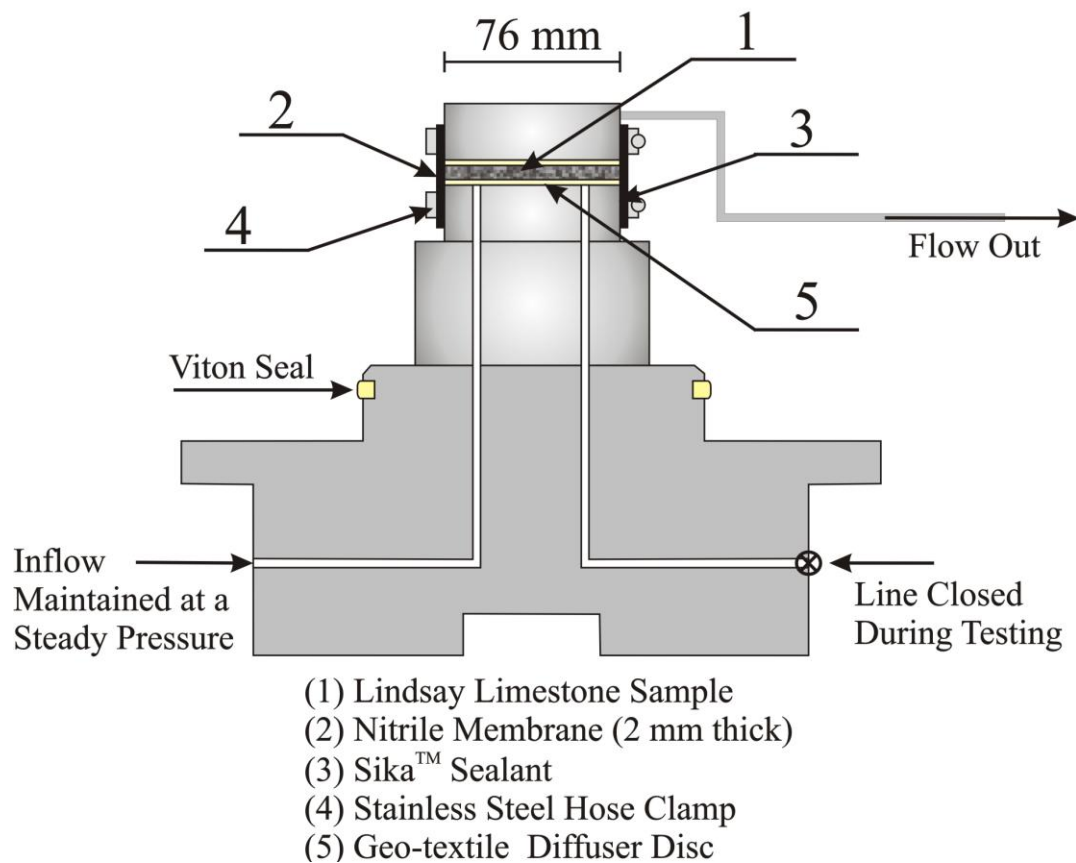


Figure 8: Detail of the sample set-up for the LCL permeability steady-state test

2.5.4 Permeability Results

The results of the steady state flow tests were consistent with the permeabilities measured previously by Selvadurai et al. (2011) and Selvadurai and Jenner (2012) on samples taken from the St Marys quarry in Bowmanville, ON, as well as those measured by Vilks and Miller (2007) and Gartner Lee Limited (2008) on specimens obtained from the site of the DGR. Based on the work by Selvadurai and Jenner (2012), it was concluded that a difference in permeability between the two material composites did exist. However, this difference was not measured during this set of experiments. It is possible that the confining pressures prevented the potential pathways between the phases from being opened by the fluid flow pressure. Table 1 shows a summary of the results. The flow rate versus time data is given in Appendix C.

Table 1: Permeability results from steady state flow tests on LCL disks

Sample Name	Thickness (mm)	Permeability, full disk ($\times 10^{-22} \text{ m}^2$)	Permeability, half disk ($\times 10^{-22} \text{ m}^2$)
DGR LCL Pilot (0)	4.1	9	n/a
DGR LCL 1	4.4	5 – 6	7 – 9
DGR LCL 2	5.0	8.5 – 13	11 – 16
DGR LCL 3	4.7	9.5 – 11	10 – 17
DGR LCL 4	5.2	6 – 10	12 – 17
DGR LCL 5	5.0	3 – 7	13 – 26

2.6 Physical Properties

The basic physical properties of the LCL were obtained using simple weighing and water evaporation techniques. These tests were conducted on samples from the proposed DGR site. Moisture content, effective porosity and wet and dry densities were obtained from the test data. The International Society for Rock Mechanics (ISRM) (1979) standard was used as a guideline for the test procedure and sample preparation.

2.6.1 Sample Preparation

Two cores of the LCL from the proposed DGR site near the Bruce Nuclear Generating Station (Figure 9) were supplied by the NWMO. They were extracted by Intera Engineering Ltd. at a recovery depth of approximately 680 m. These cores were sealed immediately after extraction from the DGR site boreholes and were considered to be fully saturated.



Figure 9: LCL cores from the DGR borehole

In order to ensure that the samples remained saturated during the machining process, the pieces not currently being worked on were kept submerged. During machining, the surface of the specimens was kept in a humid state; based on the very low permeability of the rock, it was assumed that surface de-saturation due to evaporation would occur at a slower rate than the rate at which material was removed. After being removed from their sealed packaging, each core was machined on a lathe to obtain a fixed diameter and then cut into 5 specimens of 2 different sizes (~25 mm x 75mm (3) and ~50 x 75mm (2)). The samples were further machined so that their dimensions are precisely measureable. Figure 10 shows the finished samples.

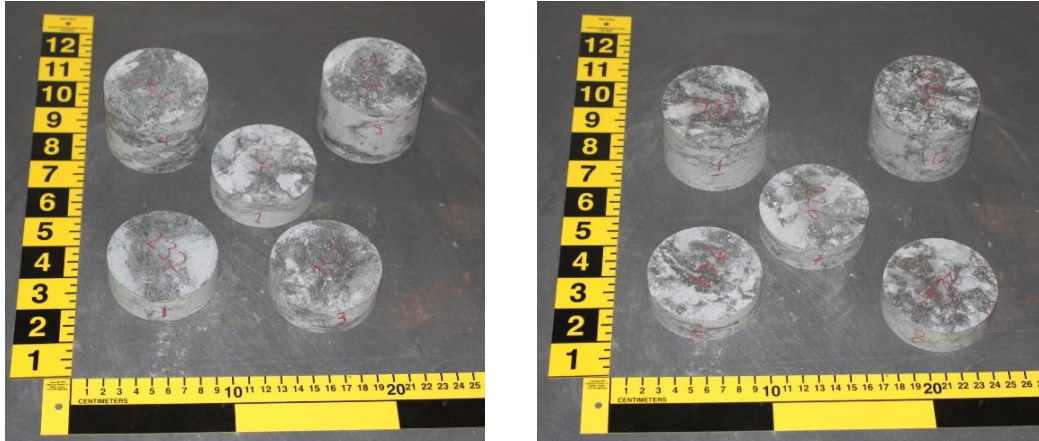


Figure 10: Test samples used to obtain the physical properties of LCL

2.6.2 Methodology

The testing was conducted following the guidelines established in the ISRM (1979) Standard. The machined samples were washed, allowed to dry and then weighed to obtain their initial saturated weight. This measurement assumes that the samples are fully saturated when taken out from the sealed packaging and that the time elapsed to machine them does not constitute a sufficiently long time for significant moisture loss to occur, given the LCL's very low permeability. The weighed samples were placed in a drying oven set at $\sim 65^{\circ}\text{C}$. The weight is recorded daily to track the progress of moisture loss. For each weighing, a set time of 10 min was used to allow the surface water to dry. In the case of LCL, the samples were subjected to the de-saturation process for 32 days.

2.6.3 Results

Table 2 shows the relevant measurements and estimated properties for the LCL samples. These results are specific to the DGR site material but can be considered as a close approximation of the properties of the material extracted from the St Marys quarry at Bowmanville.

Table 2: Physical Properties of LCL samples from the DGR site

Core 232					
Sample:	1	2	3	4	5
Total Volume (mL)	99.49	101.03	103.67	212.81	218.60
Weight of water (g)	1.26	1.55	2.09	3.56	3.17
Moisture content (% weight)	0.47	0.57	0.76	0.63	0.54
Porosity (%)	1.27	1.53	2.02	1.67	1.45
Sat. Density (g/mL)	2.69	2.69	2.69	2.69	2.68
Dry Density (g/mL)	2.68	2.68	2.67	2.67	2.67
Core 226					
Sample:	6	7	8	9	10
Total Volume (mL)	99.12	93.53	95.31	209.25	217.95
Weight of water (g)	0.99	0.87	0.94	1.58	2.11
Moisture content (% weight)	0.37	0.35	0.37	0.28	0.36
Porosity (%)	1.00	0.93	0.98	0.75	0.97
Sat. Density (g/mL)	2.69	2.70	2.69	2.70	2.69
Dry Density (g/mL)	2.68	2.69	2.68	2.69	2.68

2.7 Physical and Mechanical Properties Summary

Tables 3 to 8 provide a summary of the physical and mechanical properties of Lindsay-Cobourg Limestone that have been published in the literature. It is apparent that the tensile strength is the property that is investigated the least, whereas permeability properties have been extensively investigated.

Table 3: Summary of Young's modulus estimates for the LCL

Reference	Sample Site Location	Min (GPa)	Max (GPa)	Mean (GPa)	Median (GPa)
Golder Associates (2003)	Bowmanville	16	66	n/a	40
Gartner Lee Limited (2008)	Cobourg	10	70	31.5	n/a
Selvadurai et al. (2011)	Bowmanville	8	68	n/a	20.7

Table 4: Summary of Poisson's ratio estimates for the LCL

Reference	Sample Site Location	Min (GPa)	Max (GPa)	Mean (GPa)
Golder Associates (2003)	Bowmanville	n/a	n/a	0.3
Lam et al. (2007)	Bowmanville	0.1	0.4	0.3
Selvadurai et al. (2011)	Bowmanville	n/a	n/a	0.25

Table 5: Summary of uniaxial compressive strength estimates for the LCL

Reference	Sample Site Location	Min (MPa)	Max (MPa)	Mean (MPa)	Median (MPa)
Golder Associates (2003)	Bowmanville	25	140	109	n/a
Lam et al. (2007)	Bowmanville	22	140	72	n/a
Gartner Lee Limited (2008)	Cobourg	22	140	72	n/a
Selvadurai et al. (2011)	Bowmanville 'Cored' Perpendicular to Bedding Plane	91.4	93.6	92.5	n/a
Selvadurai et al. (2011)	Bowmanville 'Cored' Parallel to Bedding Plane	n/a	n/a	n/a	80.5

Table 6: Summary of tensile strength estimates for the LCL

Reference	Sample Site Location	Direct Tension		Brazilian Test	
		Mean (MPa)	Range (MPa)	Mean (MPa)	Range (MPa)
Lam et al. (2007)	Cobourg	1	0.04-2	6.5	3-10

Table 7: Summary of porosity estimates for the LCL

Reference	Sample Site Location	Test type	Porosity (min.) %	Porosity (max.) %
Cavé et al. (2009)	Cobourg	Water loss	1.04	3.03
Cavé et al. (2009)	Cobourg	Iodide Accessibility	1.9	3.1
Vilks and Miller (2007)	Cobourg	Water loss	1.48	2
Vilks and Miller (2007)	Cobourg	Mercury intrusion porosimetry (MIP)	1.19	1.38
Selvadurai et al. (2010)	Bowmanville	Water loss	0.97	3.4

Table 8: Estimates for permeability of LCL reported in the literature

Reference	Sample Site Location	$K_{min}(m^2)$	$K_{max}(m^2)$	$K_{median}(m^2)$
Raven et al. (1992)	OHD-1, Mississauga/Lakeview	1.02×10^{-20}	6.42×10^{-19}	3.26×10^{-19}
Raven et al. (1992)	UN-2, Darlington/Bowmanville	6.42×10^{-21}	1.36×10^{-18}	8.19×10^{-19}
Golder Associates (2003)	DDH01/02, Bowmanville	1.33×10^{-19}	4.08×10^{-18}	2.11×10^{-18}
Mazurek (2004)	In Situ Packer Tests in Vertical or Inclined Boreholes	6.42×10^{-21}	4.08×10^{-18}	n/a
Vilks and Miller (2007)	Cobourg perpendicular to Bedding Plane	$< 10^{-22}$	3.5×10^{-22}	n/a
Vilks and Miller (2007)	Cobourg parallel to Bedding Plane	1.22×10^{-22}	2.20×10^{-21}	n/a
Gartner Lee Limited (2008)	Cobourg Vertical	n/a	n/a	9.79×10^{-20}
Gartner Lee Limited (2008)	Cobourg Horizontal	n/a	n/a	9.79×10^{-19}
Selvadurai et al. (2011)	Bowmanville perpendicular to Bedding Plane	2×10^{-23}	8.80×10^{-22}	n/a
Selvadurai and Jenner (2012)	Bowmanville radial flow	1.0×10^{-21}	2.00×10^{-19}	n/a

3. Mechanical strength of Lindsay-Cobourg Limestone

Testing of geomaterials for strength and deformation can be conducted in a variety of ways. These include tension, compression, shear, flexure and torsion. In terms of characterization of failure of rock materials the two indicator properties are the compressive and tensile strength of the material; in this research, both these failure properties were determined. It bears mentioning that since these samples were obtained from the blasting quarry in Bowmanville, they may have accumulated damage. This may affect the strength properties of the LCL, most likely reducing its strength compared to rock found at the site of the DGR, especially for the tension strength measurements. However, this was deemed acceptable because the measured values would be a conservative estimate of the *in situ* strength properties. The complete data for all strength testing will be presented in a report to the Nuclear Waste Management Organization (NWMO) (Selvadurai, 2013).

3.1 Sample Preparation

Two types of samples were used for the three different tests conducted, (i.e. compressive strength, the Brazilian and plug compression splitting tests.) The samples were obtained from several slabs of LCL that were cut from a large block transported from the St Marys Quarry at specific orientations with respect to the observable bedding planes in the rock (Figure 11). The rock slabs used to obtain cores for conducting experiments associated with this research were orientated parallel and perpendicular to the bedding planes.

3.1.1 Representative volume

When dealing with heterogeneous materials such as Lindsay-Cobourg Limestone, it is necessary to choose a sample size that is representative of the bulk material. While LCL is fine-grained, it is very heterogeneous with respects to its nodular structure; therefore, a minimum sample size is required. Nodules in the sample can be as large as several centimetres; therefore any sample below this size is unlikely to be a representative volume element of the geomaterial. Two sizes of

cylindrical test specimens were used: for the compressive strength and Brazilian tension splitting test, the cylindrical specimens measured ~170 mm in height and ~85 mm in diameter. For the central cavity plug compression tests, the samples measured ~165 mm in height and ~105 mm in diameter and the cavity diameter was approximately 26 mm. The two specimen types are shown in Figure 12.



Figure 11: Slabs of LCL at various orientations

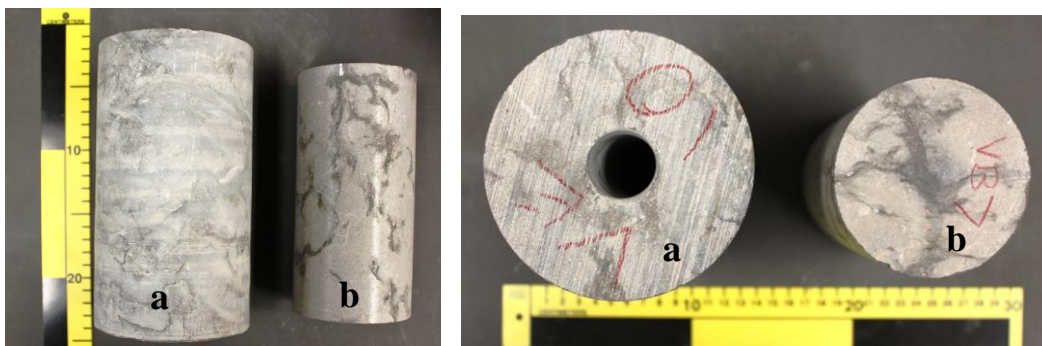


Figure 12: Test specimens a) used for central cavity expansion test; b) used for compressive strength and Brazilian splitting tests

3.1.2 Sample Preparation – Triaxial and Brazilian Tests

The samples were cored from a slab of LCL using a wet diamond coring bit with an internal diameter (ID) of 88 mm. The coring process does not generate flat edges and as such the samples needed to be machined on a lathe (Figure 13) so that contact of the specimen's surface with the membrane of the McGill-Hoek cell or with the loading surfaces of the Brazilian test frame is uniform during testing. The ends of the sample are cut by using a circular diamond saw to achieve the prescribed length. For the McGill-Hoek cell tests, the end faces of the sample were machined to obtain smooth, flat parallel surfaces. However, the samples used in the Brazilian tension splitting tests did not require machining of the end faces since the initial saw cut was sufficiently straight to comply with the ASTM C496 – 11 and D3967 standards.

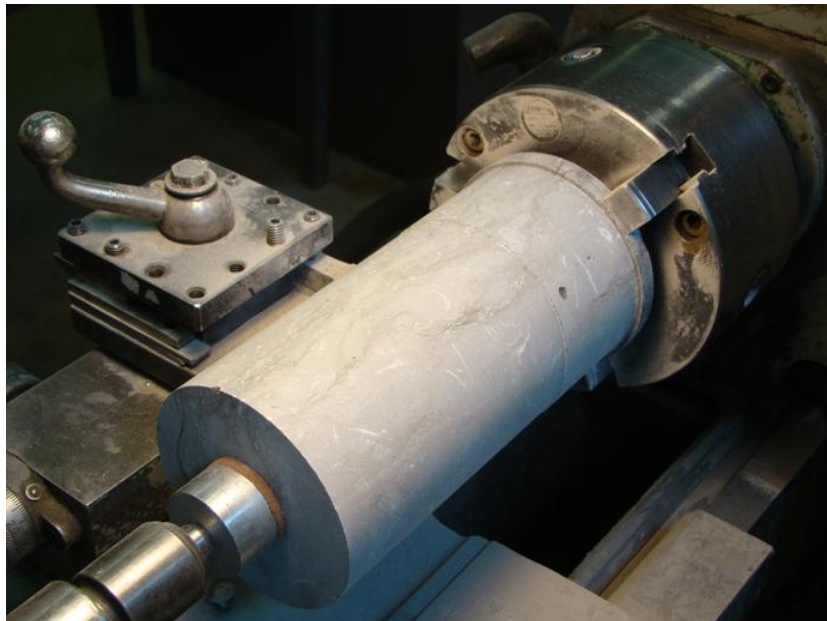


Figure 13: Machining the LCL cylinders for conducting the triaxial and splitting tests

3.1.3 Sample Preparation – Plug Compression Tests

The samples used in the plug compression tests were cored from a LCL slab using a wet diamond cutting coring bit. The central cavity is cored first and the sample is then cored out producing an annular cylinder. The central cavity is made using a corer that has an outside diameter of 25.4 mm (1 inch). The full sample is extracted using a 110 mm (4 ½ in.) OD, 105 mm (4 in.) ID corer.

The samples are then cut to a uniform length using a large circular diamond saw. The final length of a sample is 165 mm (6.5 in.) This process does not require a great deal of precise machine tool work (i.e. lathe, mill) and can be done quite rapidly. The preparation sequence is shown in Figure 14.

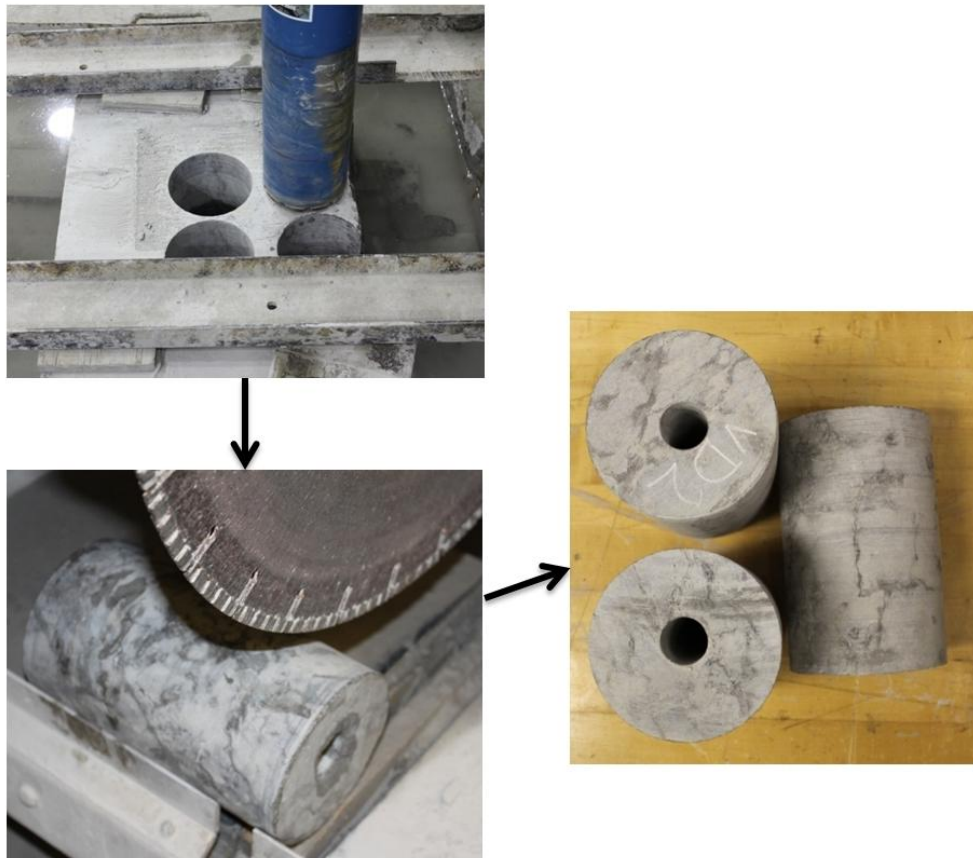


Figure 14: Preparation procedure of the plug compression tension test specimens

3.2 Compressive Strength

3.2.1 The McGill-Hoek cell apparatus

The multi axial strength tests were performed using a Hoek Cell triaxial apparatus (Figure 15). This apparatus is described by Hoek and Franklin (1968) for use in quick field testing on small cylinders. In the McGill test arrangement this test apparatus has been updated for more controlled tri-axial experiments. The cell used in these experiments allows the samples to be subjected to confining pressures of up to 60 MPa. The cell can be used to test cylindrical specimens with diameters ranging between 84 and 86 mm. The specimens tested all measured approximately 170 mm in length. The apparatus is described in more detail in Appendix A.



Figure 15: The Hoek cell

3.2.2 Methodology

The Hoek cell is assembled with its lifting rig designed by the Geomechanics Research Group and fabricated in Stekan, ON. The test sample is loaded within the cell. The test cell with the lifting rig is placed in the loading pedestal of the MTS Systems Corporation 315.03 Load Frame testing apparatus (Figure 16). This machine has a very high stiffness, which allows tests to be performed in the displacement control mode particularly as the straining progresses beyond the peak load. The cell is connected via a quick-connect valve to a GDS Instruments Inc. Controller Unit, which creates and maintains the radial stress on the sample. The axial loading is applied at a controlled rate using a computer-controlled servo-controlled system available in the MTS machine. Figure 17 shows a schematic view of the McGill-Hoek Cell assembly in the loading window of the MTS load frame.

The testing procedure first involves loading the sample to a target confining pressure in increments of 5 MPa. This is achieved by sequentially coordinating the pressure supplied by the GDS Controller Unit and the axial load applied by the MTS frame. In this loading configuration, the cylindrical test specimen is subjected to an equivalent “all round cell pressure” which is the starting point of a test. Once the desired confining load is attained, further axial loads are applied at a displacement rate of 0.1 mm/min for confining pressures between 5 and 30 MPa and a rate of 0.2 mm/min for pressures between 40 and 60 MPa. Three quasi-static loading-unloading cycles are performed to obtain (i) the peak deviatoric stress that corresponds to failure of the specimen for a given cell pressure, (ii) observe any influence of reduction in the strength of the material indicative of softening and (iii) any evidence of damage initiation as indicated in the reduction in modulus. A typical result for the principle stress (σ_1) vs. strain curve for this experiment is shown in Figure 18. Please note that for this section detailing the compressive strength of the LCL, a compression positive sign convention is used whereas a compression negative sign convention is used in the rest of this thesis when describing the tensile strength.

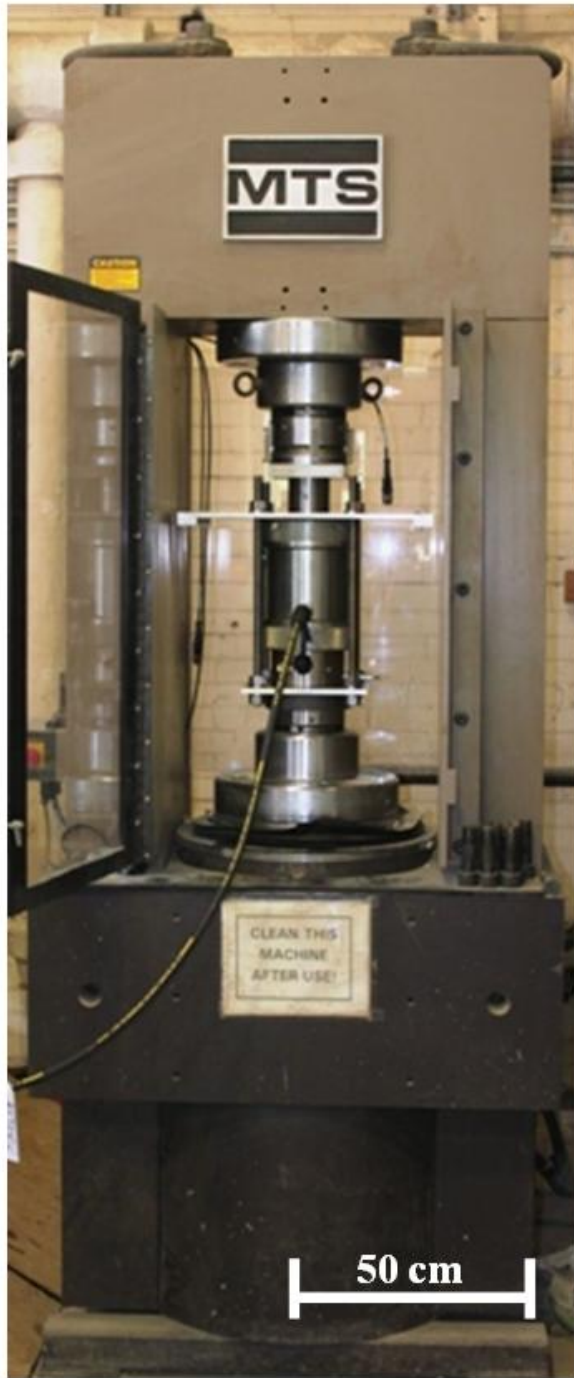


Figure 16: McGill-Hoek cell assembly in the MTS testing facility

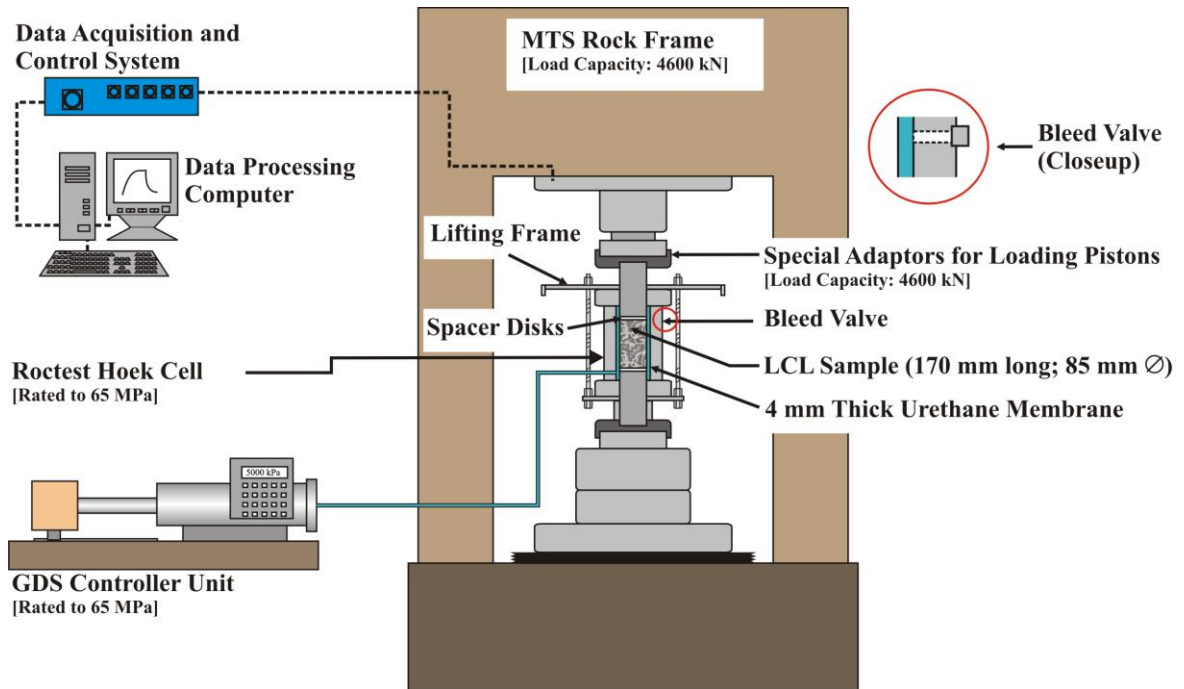


Figure 17: Schematic of the triaxial compressive strength test setup

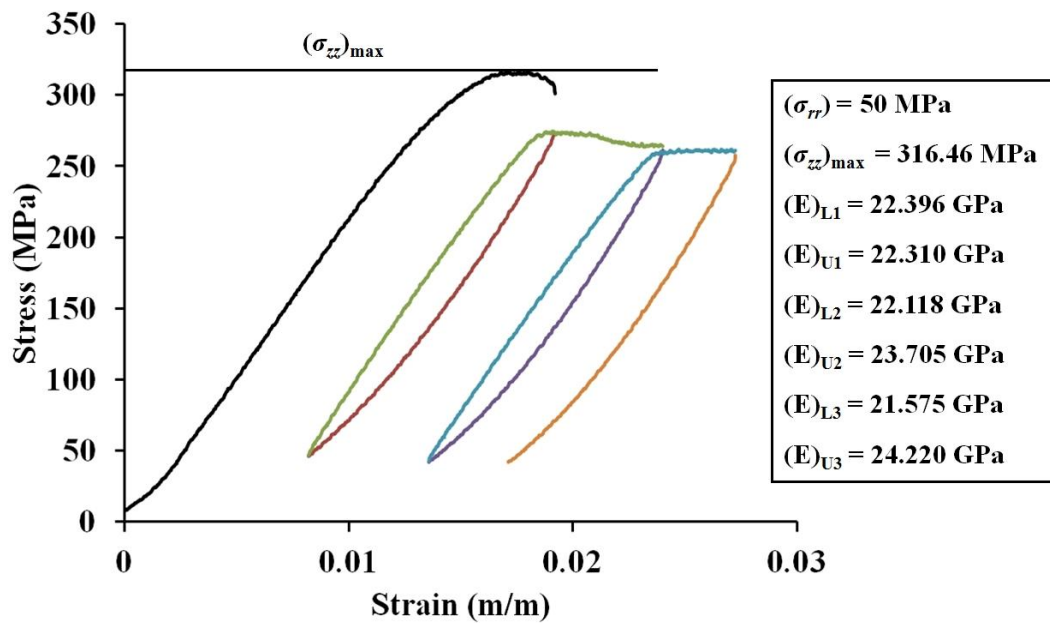


Figure 18: Typical curve for a triaxial compressive strength test on LCL

3.2.3 p vs q curve

The failure behaviour of the LCL was examined by subjecting samples of the rock to different confining pressures. This data was used to obtain a failure envelope for the rock by plotting the data on a conventional p ($= \frac{(\sigma_1 + \sigma_3)}{2}$) vs q ($= \frac{(\sigma_1 - \sigma_3)}{2}$) plot, where σ_1 is the major principle stress and σ_3 is the minor principal stress.

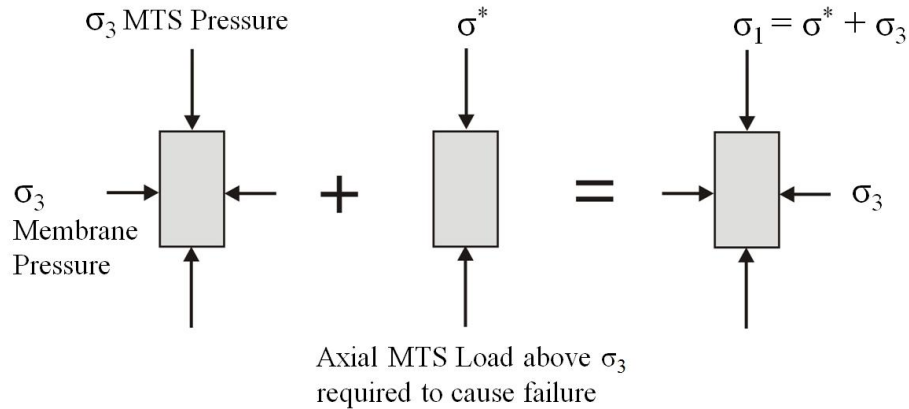


Figure 19: Progression of stress application during Hoek cell test

It is noted here that the results reported in this phase of the research is applicable to cylindrical samples whose axis are perpendicular to a nominal, observable bedding plane. Figure 20 illustrates the results of 25 experiments performed on the LCL using the McGill – Hoek cell arrangement in addition to three unconfined compressive tests. These results can be used to evaluate the Mohr-Coulomb strength parameters where $\phi = \sin^{-1}(\tan \psi)$, $c = d / \cos \phi$. From the graph shown in Figure 20, the evaluated strength parameters are $\phi = 39.6$ degrees, $c = 23.4$ MPa. These values are consistent with the Mohr Coulomb strength parameters for rock, falling between the parameters for good quality and average quality rocks (Hoek and Brown, 1997).

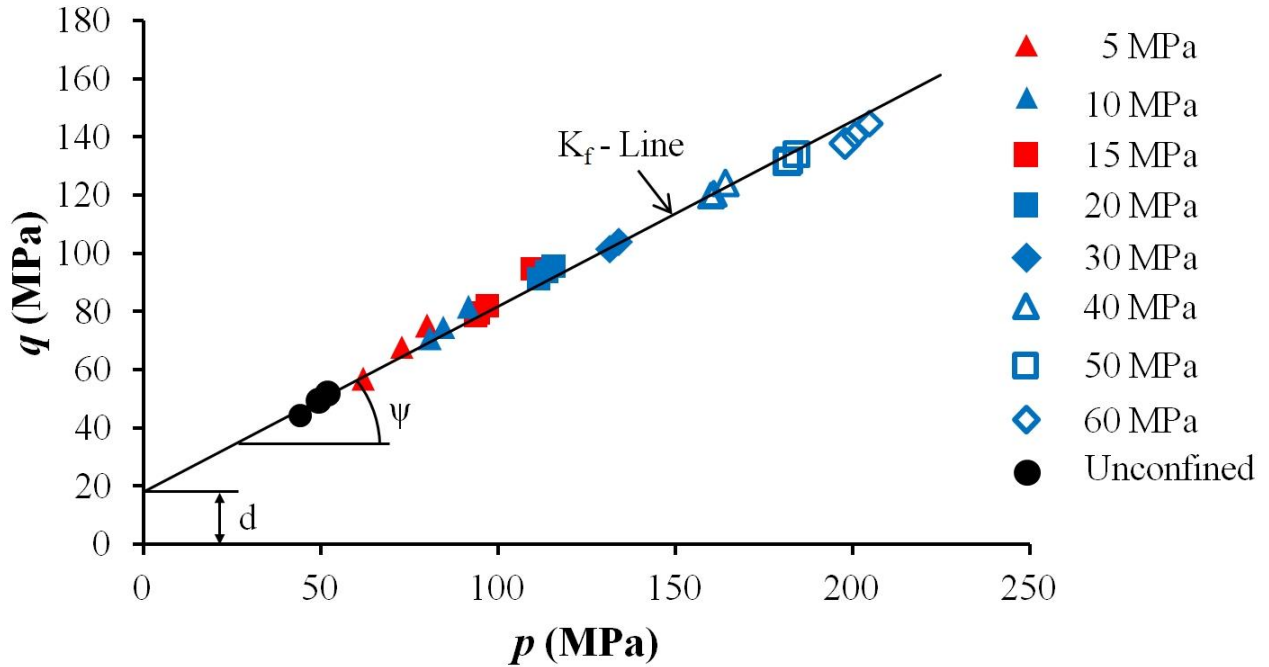


Figure 20: p vs q curve for Lindsay-Cobourg Limestone

3.3 Plug Compression Tests

3.3.1 Apparatus

The testing apparatus used for the plug compression tests involving hollow LCL cylinders consists of two steel plates with 25 mm diameter cylindrical protrusions that are used to compress a rubber cylinder or plug that will generate the radial stress at the boundary of the hollow cylinder. The apparatus is shown as a schematic in Figure 21 and its components can be seen Figure 22. The upper plate is fitted with an adapter that allows it to be connected to the upper loading platen of the MTS Load Frame; this allows for easier alignment as well as preventing the top plate from falling onto the lower part of the frame, during failure of the sample. The load is measured through a small donut-shaped load cell; the bottom plate has a nub on the opposite side of the rubber loading cylinder that fits into the hole of the load cell. The adapter plate used for the McGill Hoek cell experiment is fitted with an insert that aligns the experimental configuration. The donut load cell is connected to the MTS control computer, which continuously monitors the

axial load applied to the rubber insert, which can be related to the radial stress applied on the inner boundary of the annular cylinder.

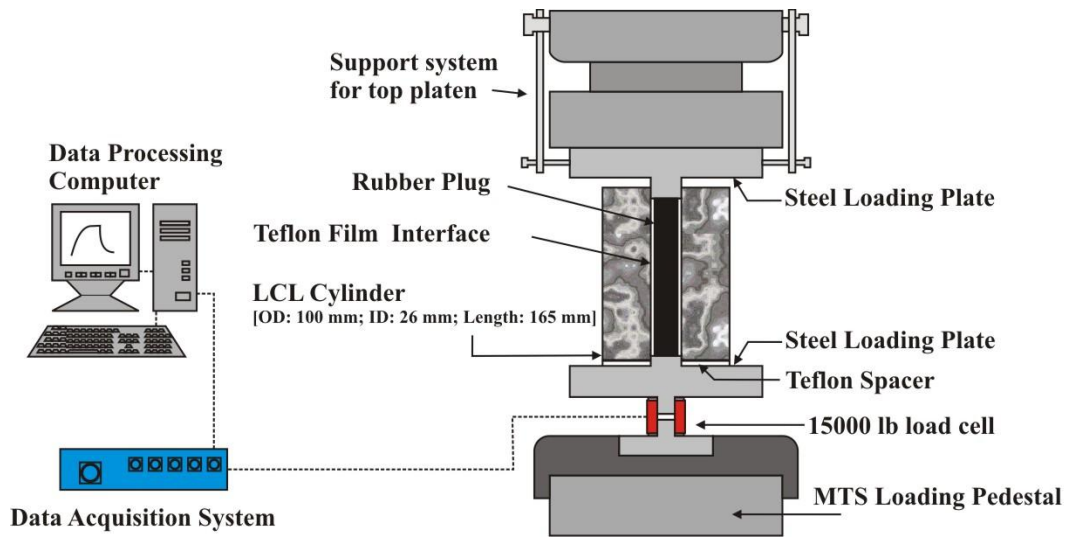


Figure 21: Schematic of the central cavity tension test set-up

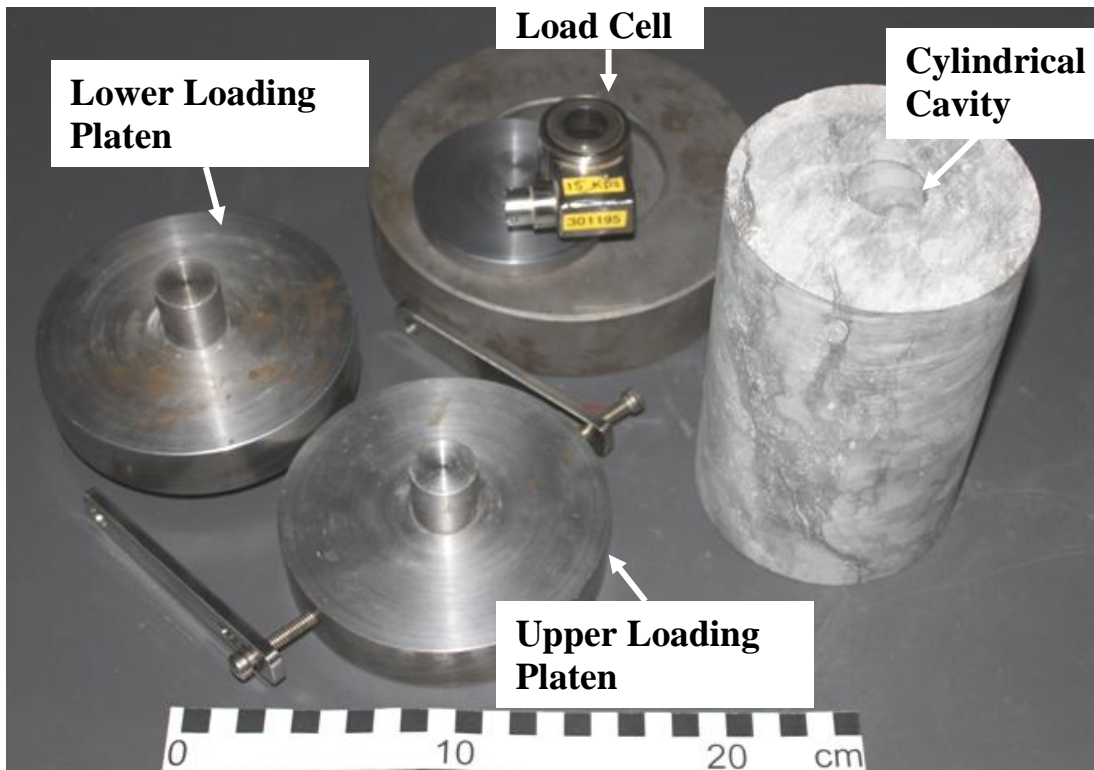


Figure 22: Dismantled plug compression test components

3.3.2 Methodology

A tensile stress state is generated in the annular cylinder during compression of the close fitting rubber plug. The rubber used in this research had a durometer value of 80 and could be regarded as being nearly incompressible. Two loading plates are used to transfer the load from the testing machine to the rubber. The interface between the rubber plug and the inner cavity of the cylinder is provided with a thin TeflonTM (PTFE) film; this will minimize any friction at the interface and ensure a relatively uniform compression over the compressed length. Once the sample is partially loaded, the base support is removed. The nominal friction resulting from the radial compression is sufficient to prevent movement of the rock and from it sliding down along the rubber to the bottom platen. In this experiment, it is explicitly assumed that there is no axial stress of appreciable magnitude induced on the test specimen through this nominal friction. This was confirmed by virtue of the fact that it was possible to adjust the position of the rock cylinder by hand during the test when it became necessary in a couple of instances.

The tests described in this thesis were performed using of the MTS 315.03 Load Frame testing apparatus (Figure 16). The testing machine is operated in the displacement control mode (i.e. the loading head in the MTS machine moves at a constant rate). Two rates are used for the plug compression test: A fast rate, 0.5 mm/min, is used to compress the rubber until sufficient radial stress is transferred to the rock. When the axial load reaches 2 kN, the displacement rate drops to a slower rate of 0.05 mm/min, until splitting failure occurs in the sample. Each segment of the test lasts approximately 10 – 15 minutes.

Since the MTS 315.03 machine is designed primarily to test the compressive strength of rock and concrete, it has a large capacity of 4600 kN. This presents a problem in accuracy when dealing with relatively small loads, such as those generated during the plug compression tests. Therefore, a small donut load cell (Appendix A) with a capacity of 70 kN is used to measure the loads generated during plug compression testing.

3.4 Brazilian Tension Splitting Tests

3.4.1 Apparatus

Figure 23 shows the Brazilian tension splitting test apparatus. It consists of a cradle and a rectangular metal bar. These pieces form the two flat surfaces that generate the load necessary to split the cylinder. In this research, an additional steel plate was required in this apparatus because the sample size used was smaller than the standard 100 mm (4 inch) samples used for concrete testing.



Figure 23: Brazilian splitting test apparatus with LCL cylinder

3.4.2 Methodology

The standard splitting test for rock (ASTM D3967 – 08) makes use of disks instead of cylinders. In view of the dominant heterogeneity of the LVL, the dimension of the sample used in a Brazilian test has to take into consideration the dimensions of the nodules. This constraint is similar to procedures adopted for splitting tests on concrete (ASTM C496M – 11), where the size sample must be in relation to the size of the aggregate. Hence, the samples used were cylinders of the same dimensions as those used in the compressive strength tests. The sample

is loaded along its length using the MTS Systems Test Frame, resulting in a diametric tensile load. A strip of compressible wood (measuring 15 mm x 3 mm x 170 mm) is used to distribute the line load over a small arc. The displacement rate used was 0.5 mm/min, which in most cases resulted in failure after ~7 min. This is consistent with the time limits presented in the test standards.

4 Analytical and Computational Modelling

4.1 Hoop Stress

When the internal boundary of a hollow cylindrical or spherical region is subjected to internal compression, it experiences what is commonly known as a hoop stress. This observation was made by G. Lamé in 1852 (Timoshenko and Goodier, 1970). This tensile stress is an important consideration in engineering design, especially when dealing with pressurized containers such as air cylinders, propane tanks and other multiple applications. In these cases, typically, the ratio of radius to thickness can be large enough (10:1 to 20:1) to use the thin wall approximation. In this instance, the stresses are defined as:

$$\sigma_{\theta} = \frac{Pr}{t}; \sigma_r = \frac{-P}{2} \quad (1)$$

where σ_{θ} and σ_r are the circumferential and radial stress respectively, P is the internal pressure, r is the radius of the vessel, and t is the wall thickness. As mentioned in chapter 3, a tension positive, compression negative sign convention is used when discussing tensile strength testing.

However, in the case of the cavity expansion resulting from plug compression, this approximation is not valid and the solution should be based on the analysis of the equations of elasticity governing three dimensional solids. The solutions of these equations are given in classical texts cited previously and will not be discussed in detail. It can be shown that when an annular elastic region is subjected to an internal pressure (compression) P , the state of stress is given by

$$\sigma_{\theta\theta} = \frac{-a^2P}{(b^2 - a^2)} \left(1 + \frac{b^2}{r^2}\right); \sigma_{rr} = \frac{-a^2P}{(b^2 - a^2)} \left(1 - \frac{b^2}{r^2}\right) \quad (2)$$

where a and b are the internal and external radii of the thick-walled cylinder. Using this result we can approximate the tensile strength of the test material,

provided the radial compression P is known. Figure 24 shows the configuration of a cross-section of an internally loaded thick walled hollow cylinder.

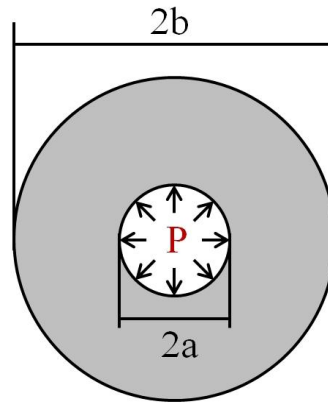


Figure 24: Uniform stress applied to the interior cavity of a hollow cylinder

4.1.1 Calculated example

If we take the measured load during the first plug test experiment, on sample HB1, we can estimate the tensile strength of the material. Given a load of 10.185 kN and a rubber plug surface area of 506.7 mm^2 we can estimate that the internal pressure to be 20.10 MPa given a Poisson's ratio of 0.49, that is typical of rubber (i.e. near incompressible.) Using the result from equation (2), given an internal diameter $a = 0.0127 \text{ m}$ and $b = 0.0508 \text{ m}$, we can estimate the circumferential stress felt at the internal face of the hollow cylinder sample as: 22.78 MPa, which is very close to the results obtained using the finite the element modeling described later in this chapter.

4.2 Brazilian test

The Brazilian splitting test also operates by using a compressive load to generate a state of tension within the test specimen. A theory of elasticity solution for a circular disc subjected to a diametral line load was first developed by Hertz in 1883 (Timoshenko and Goodier, 1970). In the case of a concentrated line load, stresses are generated at the point of application of the load, these stresses are balanced by the tensile stress state along the diametral plane. If the material has a tensile strength lower than its compressive strength, failure will occur in diametral

tension. Even when the compressing line load is distributed over a section of the circular boundary, the state of stress in the plane of the diametral compression will be largely tensile (Timoshenko and Goodier, 1970). This distribution of loads illustrated in schematic from in Figure 25. The failure load P_o can be used to estimate the tensile strength of the rock. The analytical results used for this purpose is:

$$\sigma_t = 2P_o/\pi LD \quad (3)$$

where σ_t is the tensile strength of the material, P_o is the total load applied to initiate failure and L and D are respectively, the length and diameter of the cylinder.

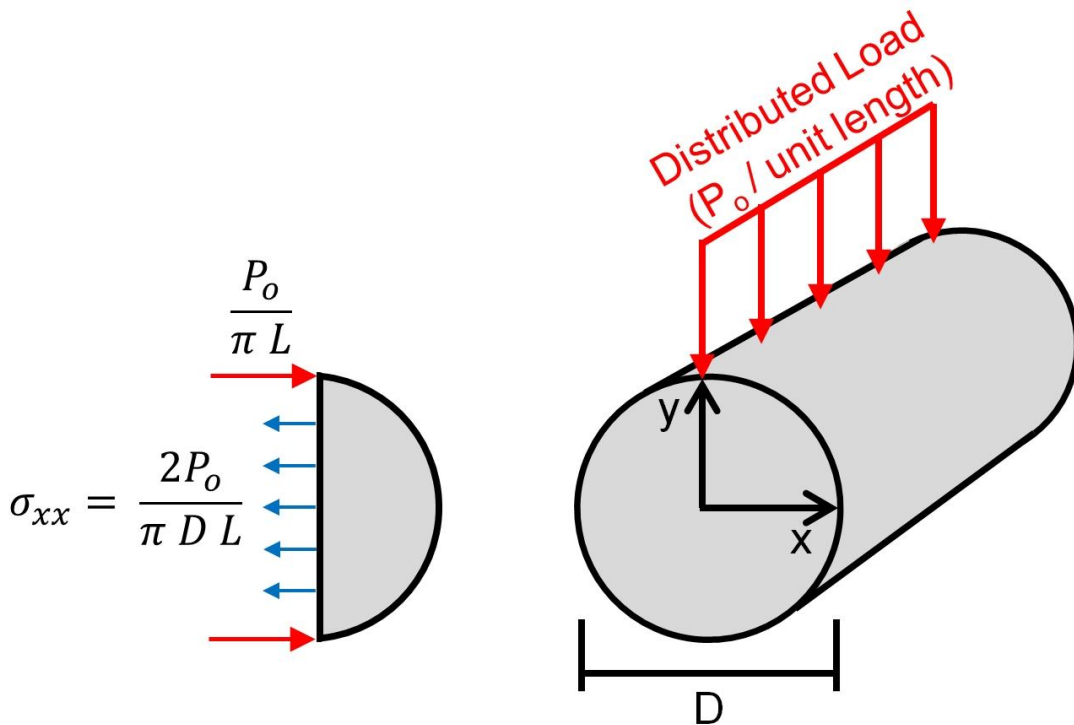


Figure 25: Stress distribution during a Brazilian splitting test

4.3 ABAQUS™ Modelling

In this section, we record the results of a stress analysis of the plug compression problem, used to estimate the tensile strength of the geomaterial. The computational approach used in the investigation employs a finite element (FE) modelling of the plug compression test. Since the plug compression test is axisymmetric, the modelling can be restricted to a model that utilizes the state of symmetry. The modelling is performed using a linear elastic analysis and all properties of the test arrangement are given plausible values applicable to steel, the LCL and the rubber plug. The physical model is shown in Figure 26; the components and dimensions are shown in a) and the boundary conditions used for the FE model are shown in b). The input parameters for the FE modelling are as follows: The steel plate ($E_S = 200 \text{ GPa}$, $\nu_{LCL} = 0.3$), the LCL ($E_{LCL} = 8 \text{ GPa}$, $\nu_{LCL} = 0.25$) and the rubber core ($E_R = 25 \text{ MPa}$, $\nu_R = 0.499$).

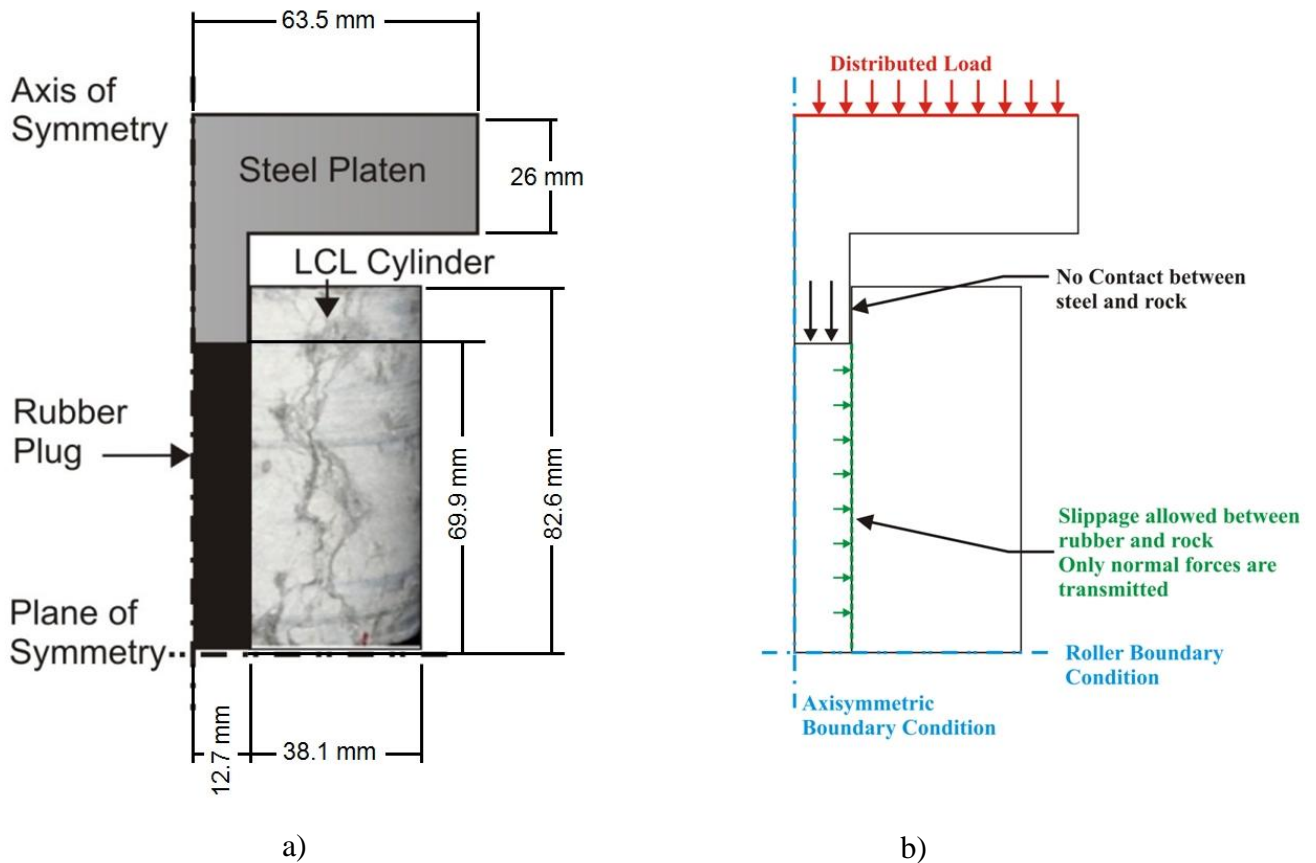


Figure 26: Physical modeling of the plug compression test
a) dimensions and components, b) boundary conditions

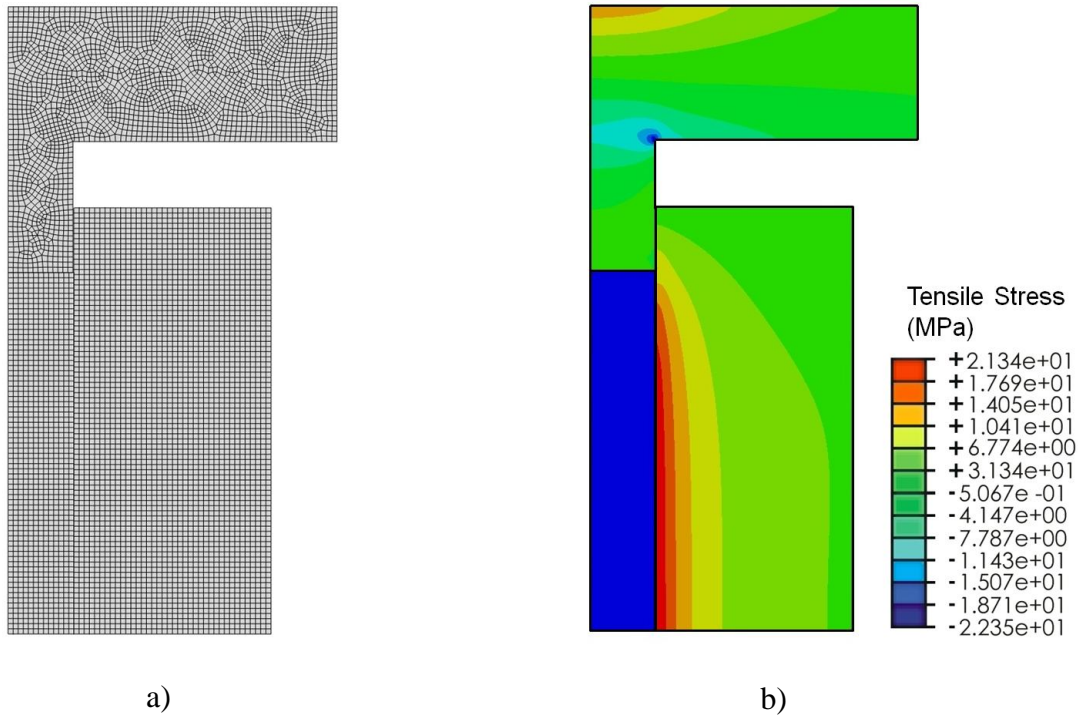


Figure 27: ABAQUS™ model for the plug compression test
a) meshing, b) simulation output for circumferential stress

Once the model is set up, the computations can be performed to determine the stress state within the annular rock core. Figure 27 shows the model mesh and a simulation output for the circumferential (tensile) stress. The colour pallet is used to show the circumferential stress developed in the sample during compression of the rubber plug. The meshing of the steel platen appears irregular because the element sizes were chosen with respect to the rock and rubber components of the model. With these element sizes the 90 degree bend causes an irregular pattern to develop during the meshing process. It may have been possible to eliminate this effect with further refining but it was not considered likely to affect the results. This modeling can easily be adapted to any dimension of cylinder. Also, a parametric analysis was conducted to examine the influence of the elastic properties of the LCL and that of the rubber on the state of hoop stress developed. It was found that the maximum hoop stress developed is relatively insensitive to variations in the properties of the rubber and LCL. From the results of the FE computations, it can be established that the maximum hoop stress applied to the

annular cylinder is approximately $(-1.075) \sigma_{\text{axial}}$, where σ_{axial} is the stress applied to the rubber plug.

4.4 Results

For the plug compression experiment, samples with observable stratifications either perpendicular or parallel to the axial direction of the test cylinders were used. While the results for the tensile strength were of the same order of magnitude, the samples cored parallel to the stratifications showed a greater variability and an overall lower strength. This is believed to be a result of the weaker planes of the darker argillaceous material being aligned with the failure plane. Table 9 shows the results of the plug compression tests. Figure 28 shows a comparison of the failure pattern of the plug compression test for both orientations.

Table 9: Results of the plug compression tension tests on LCL

	Sample	Failure stress (MPa)		Sample	Failure stress (MPa)
Perpendicular orientation with respect to axis	HB1	21.66	Parallel orientation with respect to axis	VD1	20.70
	HB2	22.73		VD2	17.39
	HB3	21.14		VD3	14.52
	HB4	22.73		VD4	19.65
	HB5	22.08		VD5	17.58
	HB6	21.34		VD6	12.88
	HB7	23.62		VD7	21.07
	HB8	12.41		VD8	18.74
	HB9	22.64		VD9	8.68
	HB10	20.93		VD10	20.80
	Mean:	21.13		VD11	22.51
		Mean:	17.68		



Figure 28: Typical failure patterns of the plug compression test samples

a) stratifications perpendicular to the axis b) stratifications parallel to the axis

In comparison, the tests conducted using the Brazilian cylinder splitting method had an overall lower tensile strength. These tests were conducted in order to try to confirm the trend seen in the plug compression tests. Fifteen samples were tested; 5 samples with stratification lines perpendicular to the axial direction and 10 samples with stratification lines parallel to the axial direction; of the latter, 5 were tested with the load applied in the direction of the stratification lines and 5 at 90 degrees from the orientation of the lines.

There was no indication of the effect of anisotropy on the results; this may be due to the manner in which fractures are generated during testing. As mentioned previously, splitting tests generate a high compressive load at the contact surfaces; this can lead to crack generation and subsequent failure of the sample before any difference in the two main components of the LCL could be observed. Table 10 shows the results of this set of Brazilian tests.

Table 10: Results of the Brazilian splitting tests on LCL

Horizontal		Vertical 0 degrees		Vertical 90 degrees	
Sample	Stress (MPa)	Sample	Stress (MPa)	Sample	Stress (MPa)
A6	7.14	VB5	6.72	VC17	6.90
A25	9.48	VC7	10.92	VC11	7.05
A21	8.20	VB13	7.88	VB8	9.27
HB66	9.04	VC14	7.65	VE2	7.46
HB33	6.10	VC6	6.80	VB12	2.80
Mean:	7.99	Mean:	7.99	Mean:	
				first 4	7.67
				all 5	6.70

It is also possible to estimate the Young's modulus of the LCL using the ABAQUSTM model. The central cavity in the LCL samples is slightly oversized due to the coring process. This means that during the early stage of the test, the load response is due only to the rubber plug as it fills the cavity. Figure 29 shows a typical load-displacement curve for a plug compression test.

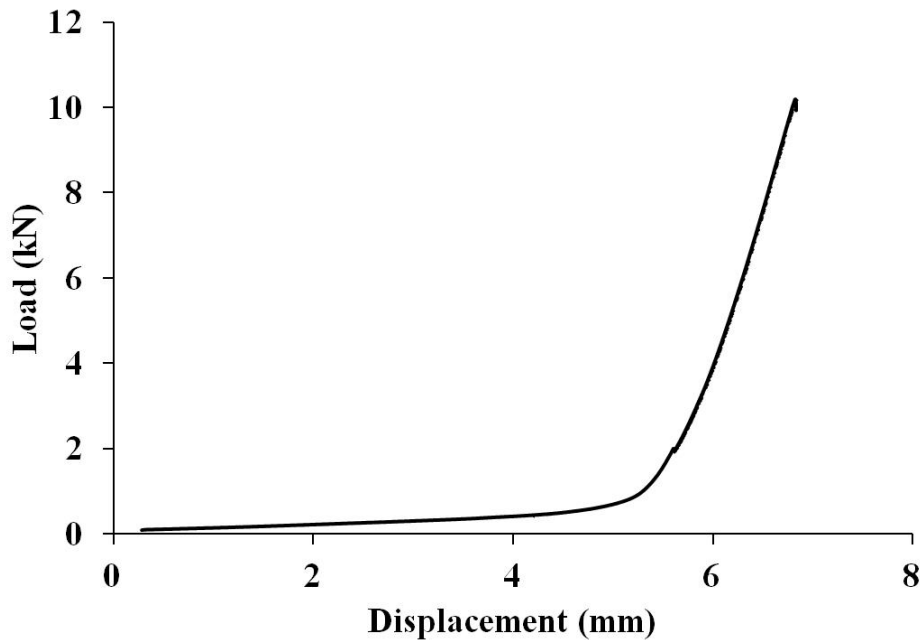


Figure 29: Typical load versus displacement curve for the plug compression test

From the first part of the curve, it is possible to estimate the deformability characteristics of the rubber. The second part of the curve corresponds to the loading of the rock specimen. The axial displacement of the load frame during the second part of the test can be used to determine the radial displacement of the rubber-rock boundary, assuming a Poisson's ratio close to 0.5 for the rubber plug. By varying the elastic modulus of the material used in the simulation, a corresponding value for the radial displacement can be found. In the case of the LCL for the plug compression tests, the Young's modulus was estimated to be 8 GPa, compared to the 20 – 24 GPa values for compressive testing. This difference in Young's moduli between tension and compression of rock has been noted in other works (Yu et al., 2005). It is important to note that this procedure will give accurate results only if the deformability characteristics of the rubber have been accurately determined and if the stress state induced does not approach the non-linear range of the material behaviour.

5. Discussion of Tensile Strength Testing

5.1 Variations in results based on methodology

There are several ways of testing the tensile strength of brittle materials such as the LCL; this research includes two different sets of experiments and methodologies for indirectly determining the splitting tensile strength of a brittle geomaterial. The other common methods of measuring tensile strength are direct tension testing, flexural testing (modulus of rupture) and point load testing (Broch and Franklin, 1972; Bieniawski and Hawkes, 1978). These methods can give different estimates of the tensile strength because each method measures the strength of the sample at a different overall stress state even if the material ultimately fails in tension. This dependence on testing procedure of the tensile strength had been studied in greater detail for concrete, and correlation factors linking the various methods are available. These correlation factors allow predictions to be made for the varying types of tensile strength (direct, point load, flexure, splitting) based on known strength values. For example, direct tension strength (f_{cr}) can be estimated from the splitting test results (f_{sp}) using the following correlation, $f_{cr} = 0.65 f_{sp}$. In addition, tensile strength can be estimated from compressive strength since it is the most commonly known parameter for concrete. (Collins and Mitchell, 1991) Further testing on LCL would be required to develop similar correlation factors. From a practical standpoint, the Brazilian splitting test is one of the preferred methods because of its relative simplicity.

5.2 Tensile strength of Lindsay-Cobourg Limestone

Tensile strength is an often overlooked property that is difficult to obtain. Although the Lindsay-Cobourg Limestone has been tested by several researchers, only one report makes mention of its tensile strength; Lam et al (2007) tested the tensile strength of LCL using both direct tension and Brazilian splitting tests. The results are reported in Table 6 in chapter 2. The Brazilian test results obtained by Lam et al. (2007) are confirmed by the current tests; the plug compression test results are higher than the ones obtained using the Brazilian test but are within the

same order of magnitude, which is consistent with the fact that both these tests measure the splitting tensile strength of the material using an indirect method. Additionally, the variation of results due to sample orientation may indicate the advantages of employing the plug compression method when a test material has a known or anticipated variability in strength due to its anisotropy.

Direct tension test were also attempted during the course of the research conducted on LCL (Figure 30); however the test preparation and execution proved difficult, and the results were considered to be somewhat unreliable. The fracture pattern of a majority of the samples tested seemed to indicate an additional moment stress present in the rock despite the use of joints in the experimental setup. The preliminary results from the tensile tests were lower than the results from the splitting tests and close to those obtained by Lam et al. (2007).

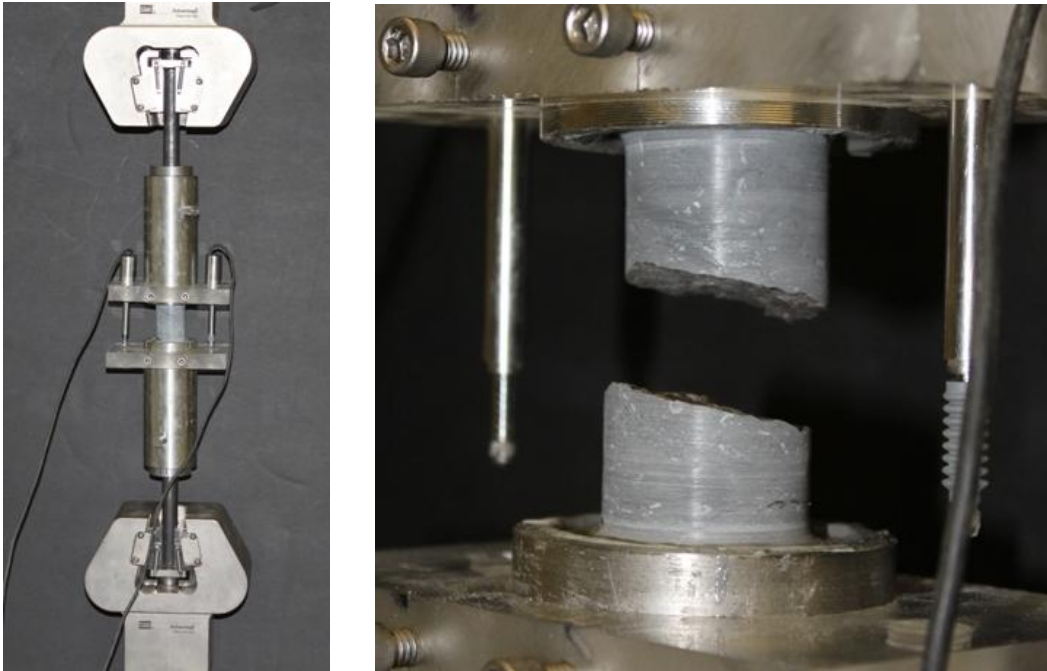


Figure 30: Direct tension testing

6. Conclusions

The accurate characterization of the mechanical and physical properties of the Lindsay-Cobourg Limestone is important to establishing the feasibility of developing a safe Deep Ground Repository for the storage of low to medium level radioactive waste products. Many of the experiments employed in the research program are modified versions of standardized tests that were adapted in view of the highly heterogeneous and highly impermeable nature of the LCL. The LCL was found to have a permeability ranging from $(5 - 26) \times 10^{-22} \text{ m}^2$ and consistent with the values found in earlier investigations reported by Vilks and Miller (2007), Gartner Lee Limited (2008), Selvadurai et al. (2011) and Selvadurai and Jenner (2012). The physical properties were found to be as follows: moisture content (%), 0.28 – 0.76; porosity (%), 0.75 – 2.02; dry density (g/mL), 2.67 – 2.69; saturated density (g/mL), 2.68 – 2.70. The triaxial testing revealed that the strength of the LCL increases linearly with confining pressure and there does not appear to be any softening at the higher confining loads. The results for the compressive strength are consistent with the ones obtained previously through testing (Golder, 2003; Lam et al., 2007; Gartner Lee Limited, 2008.) The tensile strength obtained using the plug compression method, was found to have an average value of 21.13 MPa in the case of the samples with bedding planes perpendicular to their axis and an average of 17.68 MPa in the case of the samples with bedding planes parallel to their axis. These can be compared to the results from the Brazilian splitting tests, which varied from 2.8 to 10.92 MPa with an average of 6.8 MPa, which were consistent with the results obtained by Lam et al. (2007). The Young's modulus was estimated to be 8 GPa. The plug compression tension test results in a higher measured tensile strength than the tensile strength values determined from more traditional splitting test, but it is a useful alternative for testing the tensile strength of material, giving consistent results with a simple methodology and sample preparation. It can be adapted to a greater variety of sample sizes and shapes.

6.1 Scope for Future Research

All tests associated the strength properties of LCL were conducted on samples which were in a dry or partially saturated state. The testing program can be extended to cover saturated samples. These tests should illustrate whether the mechanical properties are affected by the degree of saturation. The effect of saturation may be limited given the low porosity of the LCL. However, results obtained in Selvadurai et al. (2011) suggests that the LCL may experience internal pore pressure spikes during loading due to differential compression that results from the rock heterogeneity and the fact that these pore pressures cannot dissipate due to the LCL very low permeability. These internal pressure spikes may cause micro-cracking within the rock fabric, weakening the material. The testing can be extended to include cubical samples of the LCL. Such tests should assess the influence of saturation on the elastic modulus, Poisson's ratio and the coefficient of thermal expansion of the material. In addition, indentation testing can be done on the LCL in order to identify any differences in the elastic properties of the two primary geological species that compose the LCL. Finally, the modified Hoek cell setup allows for permeability testing; while the very low permeability of the rock does not allow intact samples to be tested, there is the potential to test the permeability characteristics of failed specimens to determine permeability of rocks in excavation damage zones and to establish the influence of confining stresses on the permeability of damaged rocks.

References

- AECOM Canada Ltd., Itasca Consulting Canada, Inc. 2011. Regional geology – Southern Ontario. *Report to NWMO*. NWMO DGR-TR-2011-15
- Alonso, E.E., T.S. Alcoverro, J. Armand, L. Borgesson, M. Chijimatsu, F. Coste, P. Jussila, M. Itamura, J. Hernelind, A. Ito, I. Kadiri, A. Kobayashi, H. Kurikami, F., L. Malinsky, Z. Maouche, V. Merrien-Soukatchoff, V. Nguyen, T. Nowak, A. Rejeb, J. Rutqvist, H. Shao, S. Sobolik, C. Stone, Y. Sugita, M. Tijani, C-F.Tsang, A.P.S. Selvadurai and S. W. Webb. 2005. The FEBEX benchmark test: case definition and comparison of modeling approaches. *International Journal of Rock Mechanics and Mining Sciences*, **42**: 611-638.
- ASTM C496 / C496M – 11. Standard test method for splitting tensile strength of cylindrical concrete specimens. *ASTM International*, West Conshohocken, PA, DOI: 10.1520/C0496_C0496M-11
- ASTM D3967 – 08. Standard test method for splitting tensile strength of intact rock core specimens. *ASTM International*, West Conshohocken, PA, DOI: 10.1520/D3967-08
- Bachu, S. and J.J. Adams. 2003. Sequestration of CO₂ in geologic media in response to climate change: capacity of deep saline aquifers to sequester CO₂ in solution. *Energy Conversion and Management*, **44**: 3151–3175.
- Banthia, N. and S. Mindess. 1989. Water permeability of cement paste. *Cement and Concrete Research*, **19**: 727-736.
- Bastiaens, W., F. Bernier, X.L. Li. 2007. SELFRAC: Experiments and conclusions on fracturing, self-healing and self-sealing processes in clays. *Physics and Chemistry of the Earth, Parts A/B/C* **32**(8–14): 600-615.
- Bataillé, A., P.Genthon, M. Rabinowicz and B. Fritz. 2006. Modeling the coupling between free and forced convection in a vertical permeable slot: Implications for the heat production of an Enhanced Geothermal System. *Geothermics* **35**(5-6): 654-682.
- Bear, J., C.-F. Tsang and G. de Marsily. 1993. *Flow and Contaminant Transport in Fractured Rock*, Academic Press, San Diego.

- Berkowitz, B. 2002. Characterizing flow and transport in fractured geological media: A review. *Advances in Water Resources* **25**(8–12): 861-884.
- Bieniawski, Z. T. and I. Hawkes, (ISRM). 1978. Suggested methods for determining tensile strength of rock materials. *International Journal of Rock Mechanics and Mining Sciences* **15**(3): 99-103.
- Bieniawski, Z. T. and M. J. Bernede, (ISRM). 1979. Suggested methods for determining the uniaxial compressive strength and deformability of rock materials. *International Journal of Rock Mechanics and Mining Sciences & Geomechanics Abstracts* **16**(2): 137
- Bill C-27. 2002. *Nuclear Fuel Waste Act*. Parliament of Canada.
- Broch, E., J. A. Franklin. 1972. The point-load strength test. *International Journal of Rock Mechanics and Mining Sciences & Geomechanics Abstracts* **9**(6): 669-676.
- Cargill, J. S. and A. Shakoor. 1990. Evaluation of empirical methods for measuring the uniaxial compressive strength of rock. *International Journal of Rock Mechanics and Mining Sciences; Geomechanics Abstracts*. **27**(6): 495-503.
- Cavé, L., T. Al, Y. Xiang and P. Vilks. 2009. A technique for estimating one-dimensional diffusion coefficients in low-permeability sedimentary rock using X-ray radiography: Comparison with through-diffusion measurements. *Journal of Contaminant Hydrology*, **103**: 1-12.
- Chapman, N. A. and I.G. McKinley. 1987. *The Geological Disposal of Nuclear Waste*, John Wiley and Sons, New York.
- Collins, M.P. and D. Mitchell. 1991. *Prestressed Concrete Structures*. Prentice Hall, New Jersey.
- Coviello, A., R. Lagioia and R. Nova. 2005. On the measurement of the tensile strength of soft rocks. *Rock Mechanics and Rock Engineering* **38**(4): 251-273.
- Dewaele, P. J., E.J. Reardon and R. Dayal. 1991. Permeability and porosity changes associated with cement grout carbonation. *Cement and Concrete Research*, **21**: 441-454.

- Fener, M., S.Kahraman, A. Bilgil and O. Gunaydin. 2005. A comparative evaluation of indirect methods to estimate the compressive strength of rocks. *Rock Mechanics and Rock Engineering* **38**(4): 329-343.
- Fredrich, J. T., K. H. Greaves and J.W. Martin. 1993. Pore geometry and transport properties of Fontainebleau sandstone. *International Journal of Rock Mechanics and Mining Sciences & Geomechanics Abstracts* **30**(7): 691-697.
- Gartner Lee Limited. 2008. DGR Supporting technical report: Phase I - geosynthesis. *Report to Ontario Power Generation*, 00216-REP-01300-00010-R00 (DOC 556).
- Golder Associates. 2003. Low level waste geotechnical feasibility study – Western waste management facility Bruce Site, Tiverton, Ontario. *Report to Ontario Power Generation*.
- Hearn, N. and R.H. Mills. 1991. A simple permeameter for water or gas flow. *Cement and Concrete Research*, **21**: 257-261.
- Hoek, E. and J.A. Franklin. 1968. A simple triaxial cell for field and laboratory testing of rock. *Transactions of the American Institute of Mining and Metallurgical Engineers*. **77**, A22- 26
- Hoek, E. and E.T. Brown. 1997. Practical estimates or rock mass strength. *Intl. J. Rock Mech. & Mining Sci. & Geomechanics Abstracts*. **34** (8), 1165-1186.
- Intera-Ltd. 1988. Inventory and assessment of hydrogeologic conditions of underground openings in sedimentary rock. *Report to Ontario Hydro*.
- ISRM. 1978. Suggested methods for determining the strength of rock materials in triaxial compression. *International Journal of Rock Mechanics and Mining Sciences & Geomechanics Abstracts* **15**(2): 47-51.
- ISRM. 1979. Suggested methods for determining water content, porosity, density, absorption and related properties and swelling and slake-durability index properties. *International Journal of Rock Mechanics and Mining Sciences & Geomechanics Abstract*. **16** (2): 141-156.
- Jenner. L. 2012. Radial hydraulic flow testing of an argillaceous limestone. *Master's Thesis, McGill University*.

- Kahraman, S. 2001. Evaluation of simple methods for assessing the uniaxial compressive strength of rock. *International Journal of Rock Mechanics and Mining Sciences* **38**(7): 981-994.
- Lam, T., D. Martin and D. McCreath. 2007. Characterising the geomechanics properties of the sedimentary rocks for the DGR excavations. *Report to Ontario Power Generation*.
- Léon Y León, C. A. 1998. New perspectives in mercury porosimetry. *Advances in Colloid and Interface Science* **76-77**: 341-372.
- Letendre. A. 2011. Permeability changes in Lindsay Limestone due to isotropic compression. *Master's Thesis, McGill University*.
- Mazurek, M. 2004. Long-term used nuclear fuel waste management – Geoscientific review of the sedimentary sequence in Southern Ontario. Technical Report TR 04-01, Institute of Geological Sciences, University of Bern, Bern, Switzerland.
- Mellor, M. and I. Hawkes. 1971. Measurement of tensile strength by diametral compression of discs and annuli. *Engineering Geology* **5**(3): 173-225.
- NWMO, 2005. Annual Report 2005: From dialogue to decision: managing Canada's nuclear fuel waste. *Report to Parliament*.
- Okubo, S. and K. Fukui. 1996. Complete stress-strain curves for various rock types in uniaxial tension. *International Journal of Rock Mechanics and Mining Sciences & Geomechanics Abstracts* **33**(6): 549-556.
- Raven, K., K.S. Novakowski, R.M. Yager and R.J. Heystee. 1992. Supernormal fluid pressures in sedimentary rocks of southern Ontario: Western New York State. *Canadian Geotechnical Journal*, **29**: 80-93.
- Selvadurai, A.P.S. 1996. The settlement of a rigid circular foundation resting in a halfspace exhibiting a near surface elastic non-homogeneity. *International Journal for Numerical and Analytical Methods in Geomechanics*, **20**: 351-364.
- Selvadurai, A.P.S. 2004. Stationary damage modelling of poroelastic contact. *International Journal of Solids and Structures*, **41**: 2043-2064.

- Selvadurai, A.P.S. 2006. Gravity-driven advective transport during deep geological disposal of contaminants, *Geophysical Research Letters*, **33**: L08408. (doi:10.1029/2006GL025944).
- Selvadurai, A.P.S. 2007. The analytical method in geomechanics. *Applied Mechanics Reviews*, **60**: 87-106.
- Selvadurai, A.P.S. 2009. Influence of residual hydraulic gradients on decay curves for one-dimensional hydraulic pulse tests. *Geophysical Journal International* **177.3**: 1357-1365.
- Selvadurai, A.P.S. 2013. Mechanical and physical properties of the Lindsay-Cobourg Limestone. *Interim Report to the Nuclear Waste Management Organization*, ON.
- Selvadurai, A.P.S. and T.S. Nguyen. 1995. Computational modelling of isothermal consolidation of fractured porous media. *Computers and Geotechnics* **17**(1): 39-73.
- Selvadurai, A.P.S. and T.S. Nguyen. 1997. Scoping analyses of the coupled thermal-hydrological-mechanical behaviour of the rock mass around a nuclear fuel waste repository. *Engineering Geology*, **47**: 379-400.
- Selvadurai, A.P.S. and A. Glowacki. 2008. Permeability hysteresis of limestone during isotropic compression. *Ground Water*, **46**: 113-119.
- Selvadurai, A.P.S., A. Letendre and B. Hekimi. 2011. Axial flow hydraulic pulse testing of an argillaceous limestone. *Environmental Earth Sciences*, DOI 10.1007/s12665-011-1027-7
- Selvadurai, A.P.S. and Jenner, L. 2012. Radial flow permeability testing of an argillaceous limestone. *Ground Water*, doi: 10.1111/j.1745-6584.2012.00932.x
- Sonmez, H., E. Tuncay, and C. Gokceoglu. 2004. Models to predict the uniaxial compressive strength and the modulus of elasticity for Ankara Agglomerate. *International Journal of Rock Mechanics and Mining Sciences* **41**(5): 717-729.
- Thury, M. 2002. The characteristics of the Opalinus Clay investigated in the Mont Terri underground rock laboratory in Switzerland. *Comptes Rendus Physique* **3**(7-8): 923-933.

- Timoshenko, S.P. and J.N. Goodier. 1970. *Theory of Elasticity, 3rd Edition*. McGraw-Hill Book Company, New York.
- Vilks, P. and N.H. Miller. 2007. Evaluation of experimental protocols for characterizing diffusion in sedimentary rocks: Atomic Energy of Canada Limited. *Nuclear Waste Management Division Report TR-2007-11*. Toronto, Ontario.
- Yu, X., C.D. Da Gama, Y. Na, Q. Wang and Q. Xie. 2005. Deformation behaviour of rocks under compression and direct tension. *Journal of The South African Institute of Mining and Metallurgy* **105**(1): 55-62.

Appendices

Appendix A: Experimental Facilities

A – 1: Hoek Cell

The Hoek cell was developed in 1968 to perform quick triaxial tests in the field. The initial apparatus was designed to employ small samples and weighed no more than 10 lbs. (Hoek and Franklin, 1968) The same basic design was scaled up to accept larger samples such as the ones used in the triaxial testing sequences. Additionally, since the Hoek cell is being used in conjunction with the GDS Controller and the MTS 315 Load Frame, it is now possible to conduct more controlled experiments than with the the device supplied by Roctest [<http://www.roctest-group.com/>]. The main issue is placing the cell in the test frame; because of the increased size, weight and height of the Hoek cell and narrowness of the load frame, it was necessary to design a lifting system for the cell. The system was designed under the supervision of Professor Selvadurai and fabricated at Stekan, ON. Figure A - 1 shows the different components of the Hoek Cell apparatus in position within the MTS Test Frame. In addition to the lifting harness, two hardened steel adaptors were supplied by Roctest, to be used at the upper and lower loading points of the MTS frame, to ensure correct alignment of the cell.

The Hoek cell can handle radial pressures up to 64 MPa (10000 psi) and is operated in conjunction with the GDS Controller unit and MTS Load Frame. It can be used with other pumps and load frames with suitable adaptors. The Hoek cell can also accommodate strain gages on the test specimens if special platens with flattened access regions are incorporated to allow the leads to exit. The modified Hoek design can also be used to test the permeability of rocks and/or other porous material under triaxial conditions.

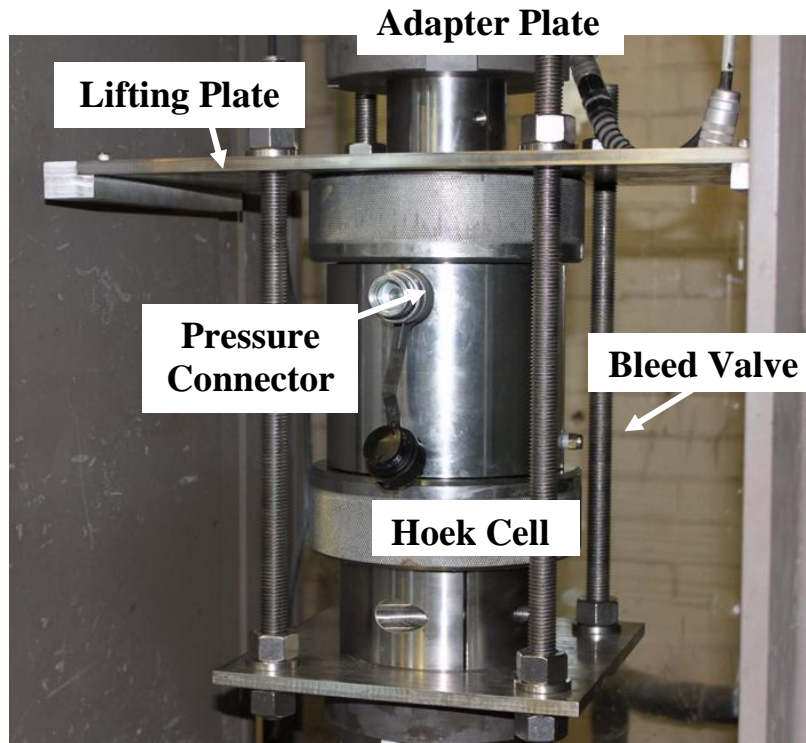


Figure A - 1: Hoek cell loading frame

A – 2: GDS Controller Unit

In order to supply pressure at a constant value to the tri-axial cells used in the Environmental Geomechanics Laboratory, a high precision, high pressure pump is needed. GDS Instruments Inc. of the UK [<http://www.gdsinstruments.com/>] manufactures a controller unit (ADVDP), which is a microprocessor-controlled screw pump that is driven by a stepper motor. The controller unit directs a servo-controlled, single piston pump and can supply and maintain pressures up to 64 MPa (10 000 psi.) The controller unit has a volume accuracy of 0.02 mm³ and a pressure accuracy of 0.01% at full scale output. The volume capacity of the piston is 207 mL. The servo unit is configured to use high damping when pressurizing; this ensures that there is no overshoot in the target pressure, but also results in a slow rate of pressurization / depressurization. This can present a problem when the Hoek cell apparatus is used for strength testing, as the controller unit will have to react rapidly to the volume changes in the sample that can occur post failure particularly during tri-axial compression tests. The pump can be used with different pressurizing fluids; in the case of the GDS cell, water is used as the fluid

and for the Hoek cell arrangement, Enerpac® HF-102 hydraulic fluid is used. Figure A - 2 shows the GDS ADVDPCC unit.

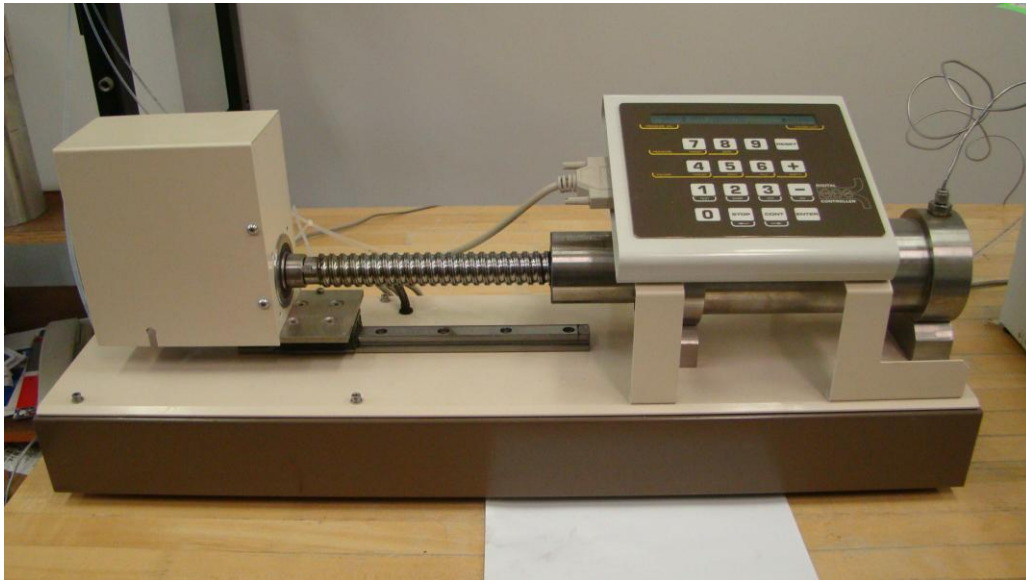


Figure A - 2: GDS controller unit

A – 3: MTS 315.03 Load Frame

The MTS 315.03 Load frame is manufactured by MTS Systems of Minneapolis, MINN, USA [<http://www.mts.com/>]. It is suitable for testing brittle materials such as concrete and rock. The load frame is characterized by its high stiffness, which reduces the energy stored in the frame thus reducing the energy released during the sudden failure of brittle materials. Parallel alignment of the loading points is ensured by a ball joint located at the cross-head. The test space is large enough to accommodate most sample sizes and large test fixtures such as the McGill-Hoek Cell.

The Load Frame uses servo controlled hydraulics to generate the axial load. The system is cooled by water. The servo-systems are operated by a controller unit that can be connected to a computer or can be operated independently. The McGill test frame is operated using the dedicated MTS software provided with the installation. This software allows for customization of test procedures (i.e.

loading rates, failure detection, number of cycles, etc.), the setting of safety limits, data recording format, and many other options.

Although the system is typically employed for compressive testing, the actuator can also be used in tension. The entire piston assembly can travel up to 100 mm. The load is measured by calculating the differential pressure between the hydraulics that power the load frame. The load is accurate to within $\pm 1\%$ of the calibrated range at loads above 1000kN. Displacement is measured by an internal LVDT which is designed and calibrated to correctly read the full scale travel of the apparatus in order to provide complete positioning control. Lastly, the system can be adapted to receive, record and act upon external inputs as well as return output signals for external applications.

A – 4: GDS Tri-axial Cell

This triaxial cell was manufactured by GDS Instruments Inc. of the UK [<http://www.gdsinstruments.com/>]. It is made of 316 grade stainless steel. The confining pressure (i.e. minimum principal stress σ_3) is applied isotropically, and a deviatoric load can be applied independently in the axial direction. The cell is composed of 4 main parts: the shell, the base pedestal, the clamp rings and the confining ring. To assemble the apparatus, the shell is lowered onto the base pedestal, the clamp rings are placed to hold the two parts in place and the confining ring is slipped onto the clamp rings to fix their position.

Figure A - 3 shows the external view of the apparatus as well as an internal schematic of the GDS cell. The cell can be pressurized up to 64 MPa (10 000 psi) and can apply deviatoric loads up to 250 kN. The base contains the connections that allow for cell pressurization as well as flow in and out of the sample. The cell can be used with different fluids, but in this research, tap water was used as the pressurizing fluid and distilled-deaired water was used as the permeating fluid.

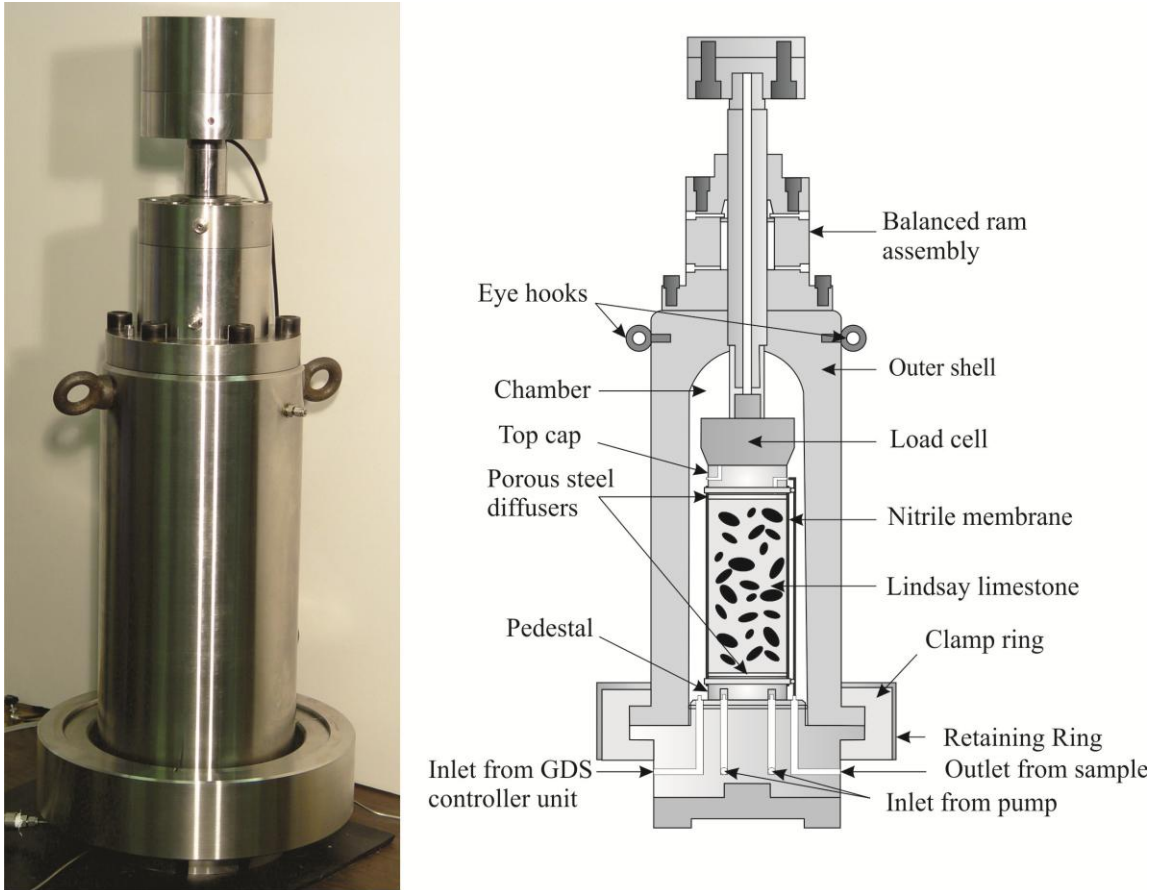


Figure A - 3: GDS triaxial cell

A – 5: Quizix QX-6000HC Dual Piston Pump

A high precision pump is used to supply water into the sample during the permeability testing. The Quizix QX-6000HC, manufactured by Vindum Engineering [[www.vindum.com/Pump Systems.html](http://www.vindum.com/Pump%20Systems.html)], is a dual piston positive displacement pump (Figure A - 4). It has many different modes of operation. In the dual piston constant flow mode, it can accurately deliver high flow rates of 50 ml/min to low flow rates of 0.00034 ml/min. It can also be operated in constant a pressure mode, delivering and maintaining a prescribed pressure. The Quizix pump can handle pressures up to 41 MPa and can be controlled from a panel or by the Pumpworks software supplied Vindum Engineering. The software can be used to program test cycles as well as recording the flow through the pistons and can deal with extremely low flows, as was required for with the steady state testing of the LCL samples.

Additional Technical Information

- Flow Rate Accuracy: +/- 0.1% of set flow rate
- Volume Accuracy: +/- 0.1% of volume pumped
- Pressure Accuracy: +/- 0.2% of Full Scale
- Pressure Resolution: 0.024 psi (0.004% of Full Scale)
- Pressure Control Accuracy (Typical): +/- 1.2 psi (0.02% of Full Scale)
- Temperature Rating: 10 to 50°C (50 to 120°F)

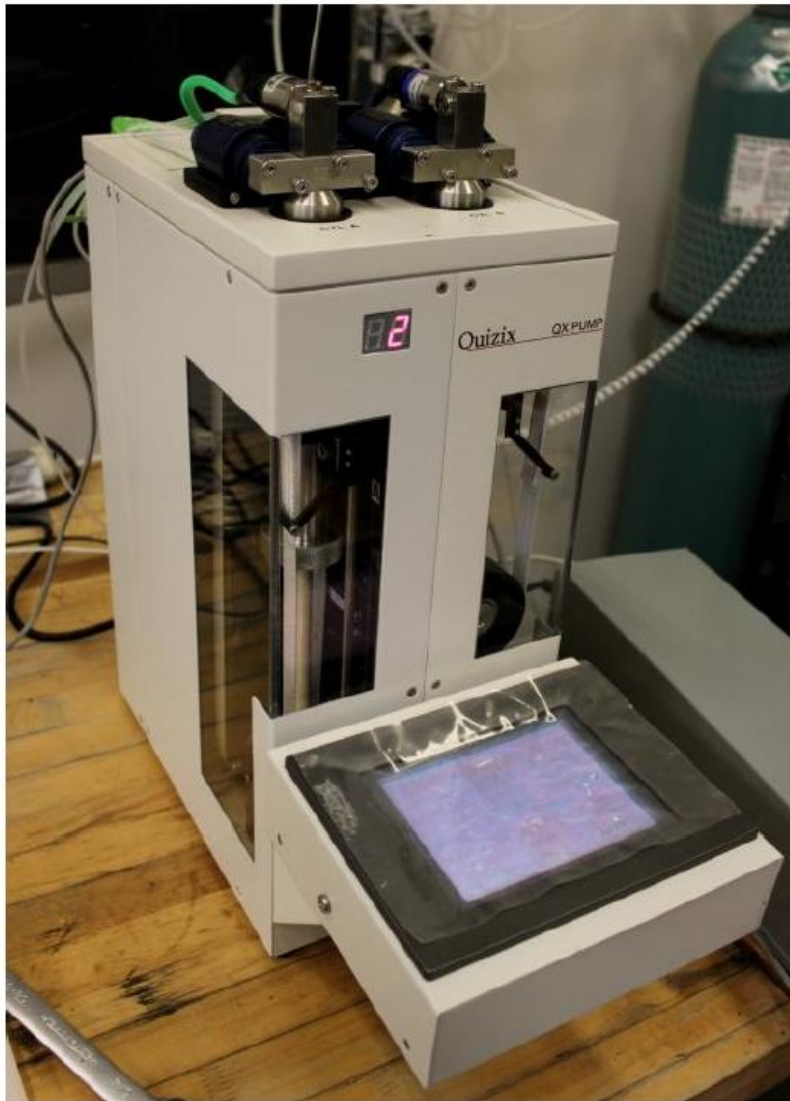


Figure A - 4: Quizix dual piston pump ([www.vindum.com/Pump Systems.html](http://www.vindum.com/Pump%20Systems.html))

A – 6: Sensotec Model TH EJ load cell

This donut load cell, shown in Figure A - 5, is used to accurately measure the load applied during the plug compression tension tests. It was manufactured by Sensotec (now a division of Honeywell [<https://measurementsensors.honeywell.com/Pages/default.aspx>]). It is designed to measure loads up to 67 kN (15 kips). The load cell was integrated into the MTS control system and calibrated so that the servos that control piston movement use the donut cell readings for control decisions, such as maximum load. This allows for a greater level of control and apparatus safety, given the high load potential of the MTS load frame.

Additional Technical Information

- Accuracy 0.5 %
- Linearity (max.) ± 0.25 % full scale
- Hysteresis (max.) ± 0.25 % full scale
- Non-repeatability (max.) ± 0.1 % full scale
- Output (tolerance) 2 mV/V (nominal)



Figure A - 5: Sensotec 67 kN (15 kips) donut load cell

A – 7: Blue M drying oven

A drying oven (Figure A – 6) was used to de-saturate the samples used for water content, porosity and density testing. This oven was manufactured by Blue M, a division of General Signal, now owned by SPX [<http://www.spx.com/en/>]. The oven can supply temperatures ranging from 40 °C to 200 °C. It is designed to dry wood, soils, aggregate, concrete and rock. This oven is designed to operate continuously, making it ideal for drying the LCL given the long periods of time required to completely de-saturate the low permeability limestone.



Figure A - 6: Drying oven

A – 8: Saturation Chamber

In order to test for the physical properties, as well as when preparing the samples for permeability tests, it is necessary to saturate the pore space with distilled water. A saturation chamber was used to achieve this. The sample is subjected to a high vacuum (-95 KPa), causing the pore air to be expelled and replaced by water. Figure A - 7 shows the equipment being used to saturate the LCL samples for porosity and density measurements. It is possible to utilize a vibrating plate to enhance the saturation procedure. However, this is usually done on larger samples than the ones employed in research. In order to ensure proper saturation, the samples are only partially submerged at first so that any the trapped air has a path to exit the rock matrix before water enters into the pore space by a combination of capillary action and suction.

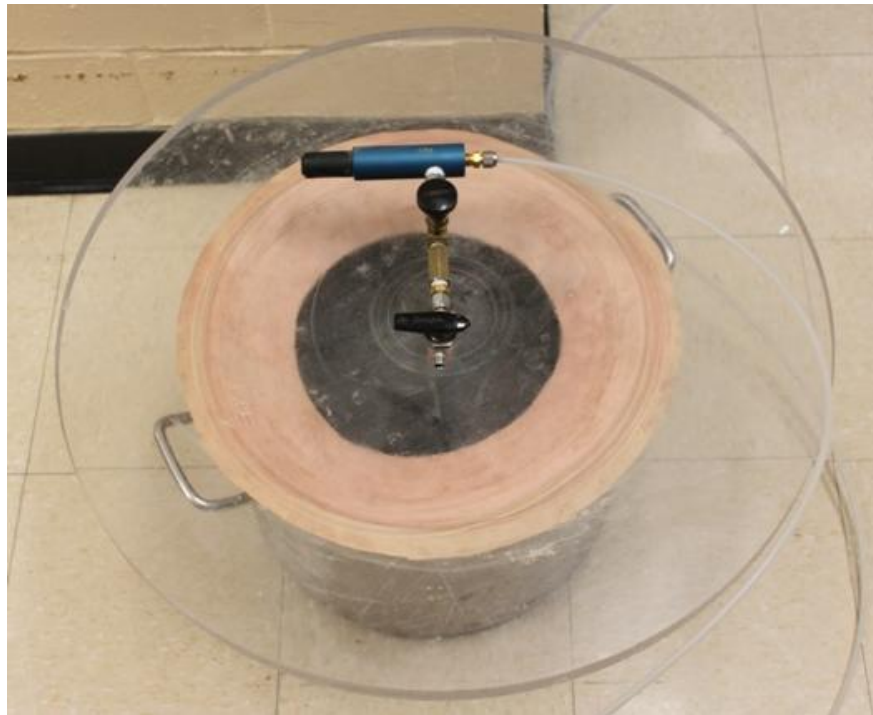
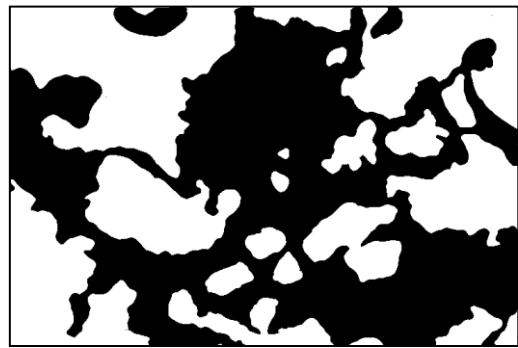
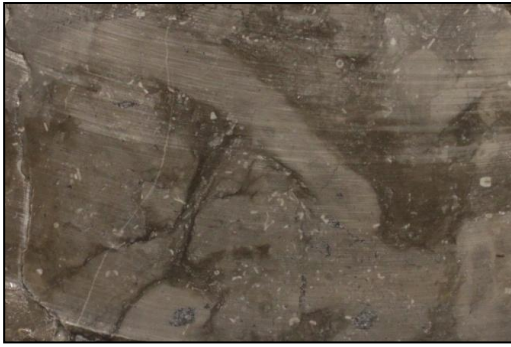


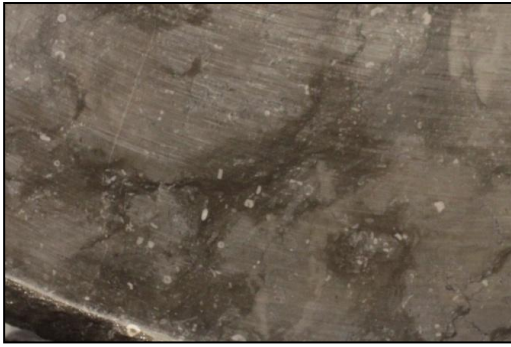
Figure A - 7: Saturation chamber

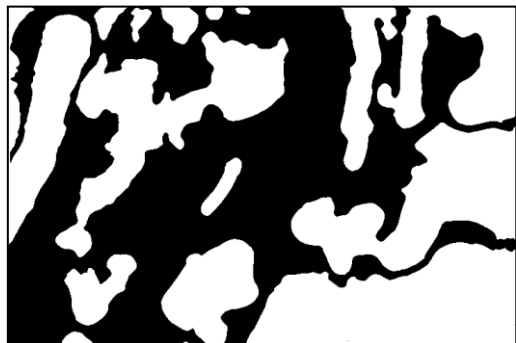
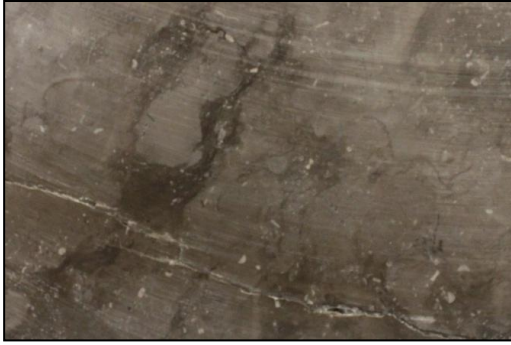
Appendix B: Photographic Records and the Digitized Images

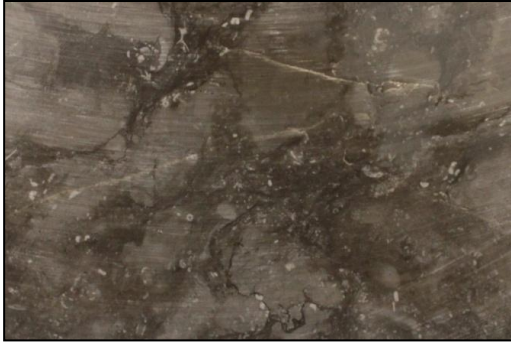


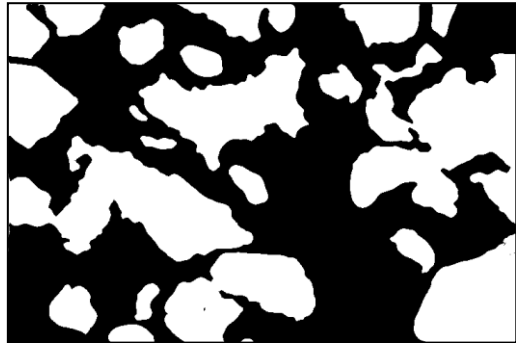
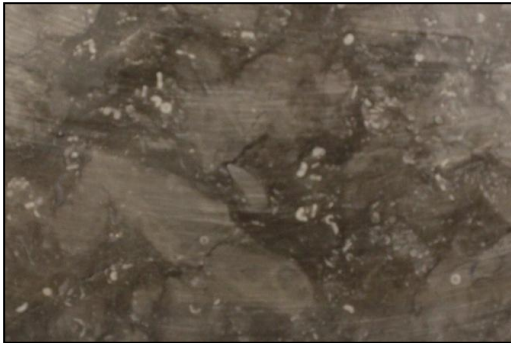








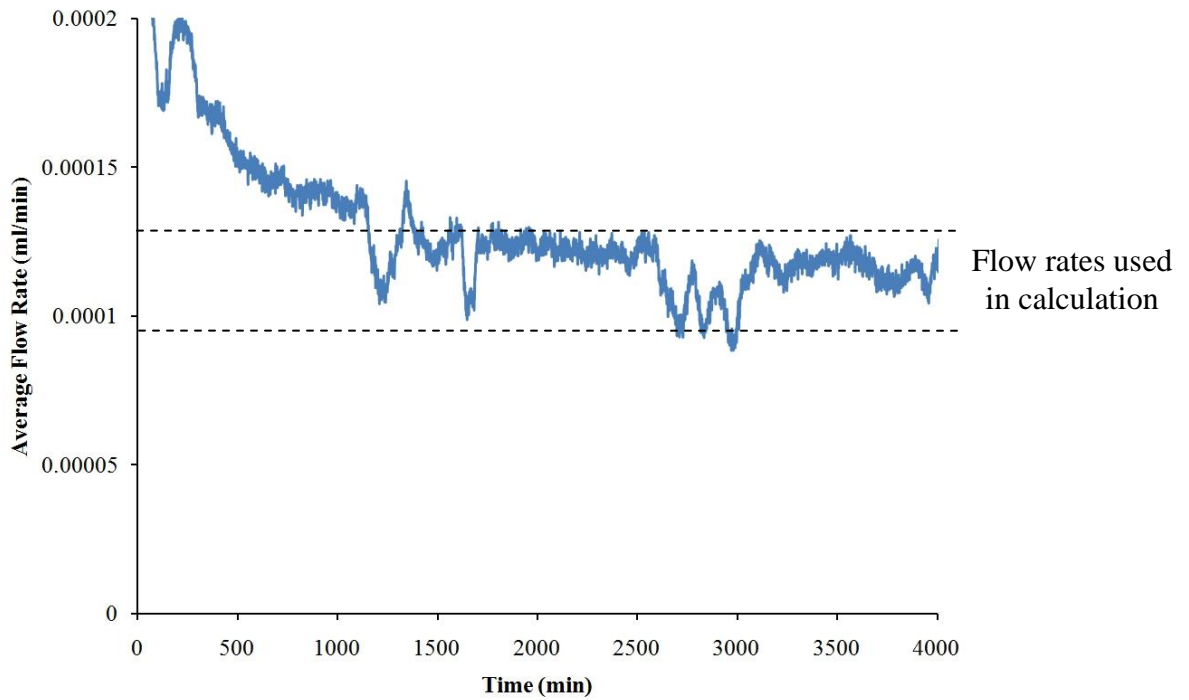




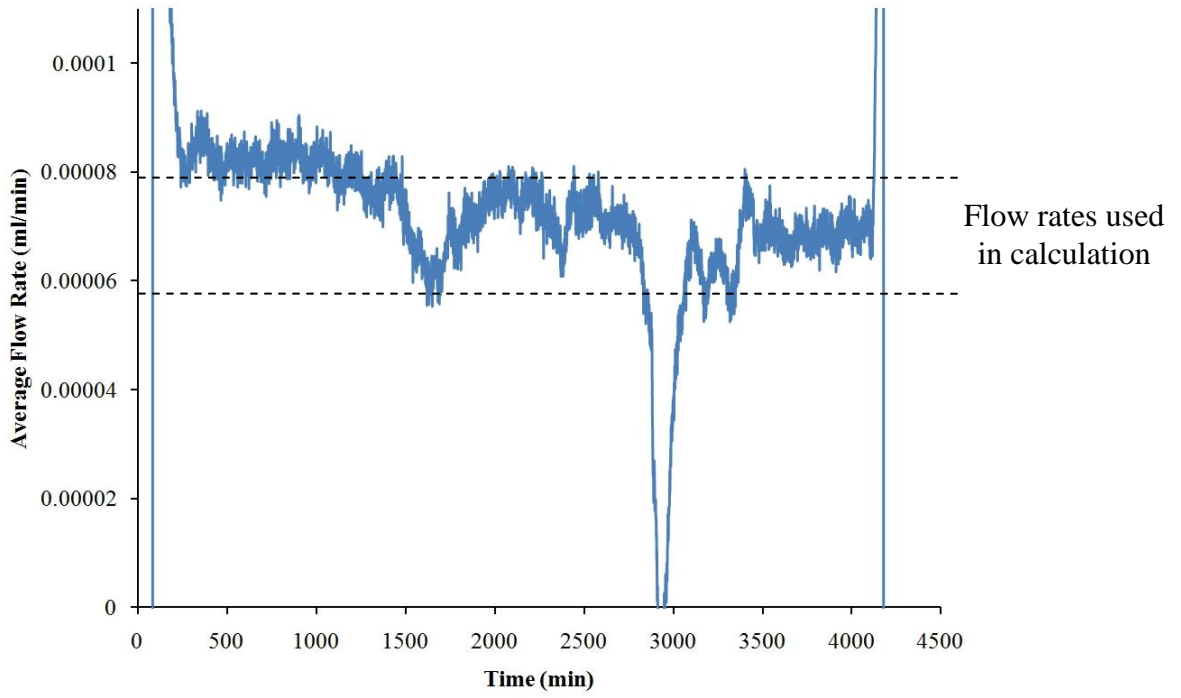


Appendix C: Steady State test data

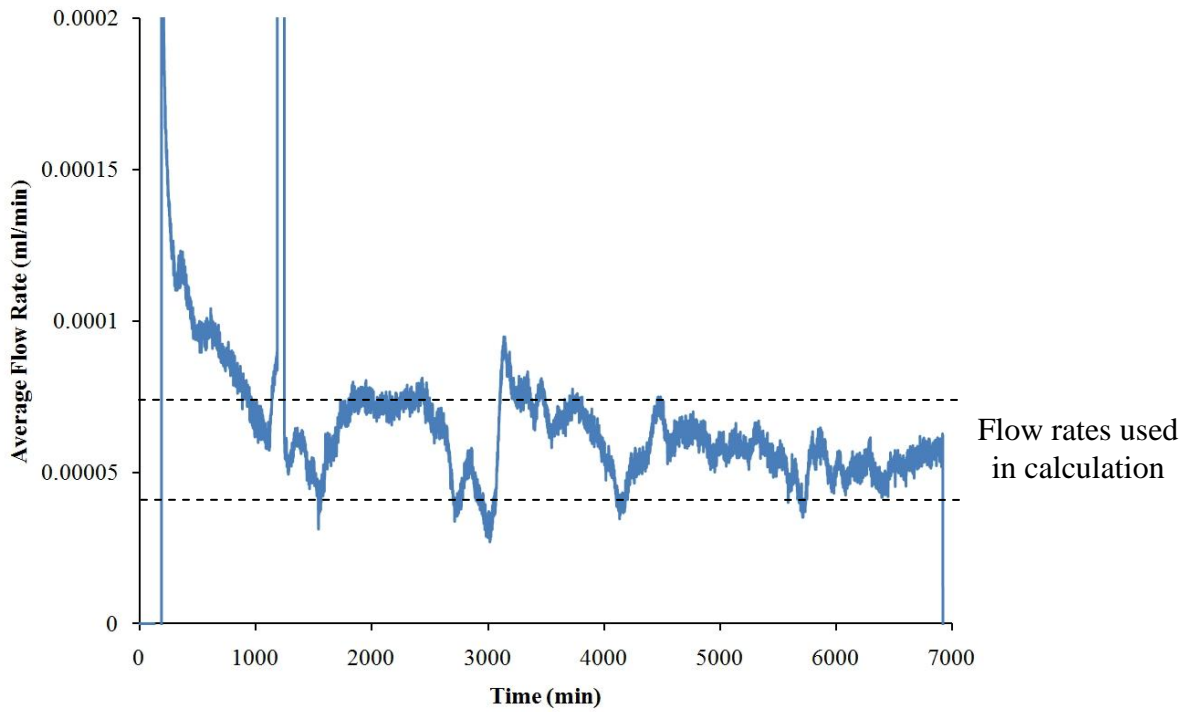
DRG LCL Disk 0 - full surface (dimensions: 75 mm diameter and 4.1 mm thickness)



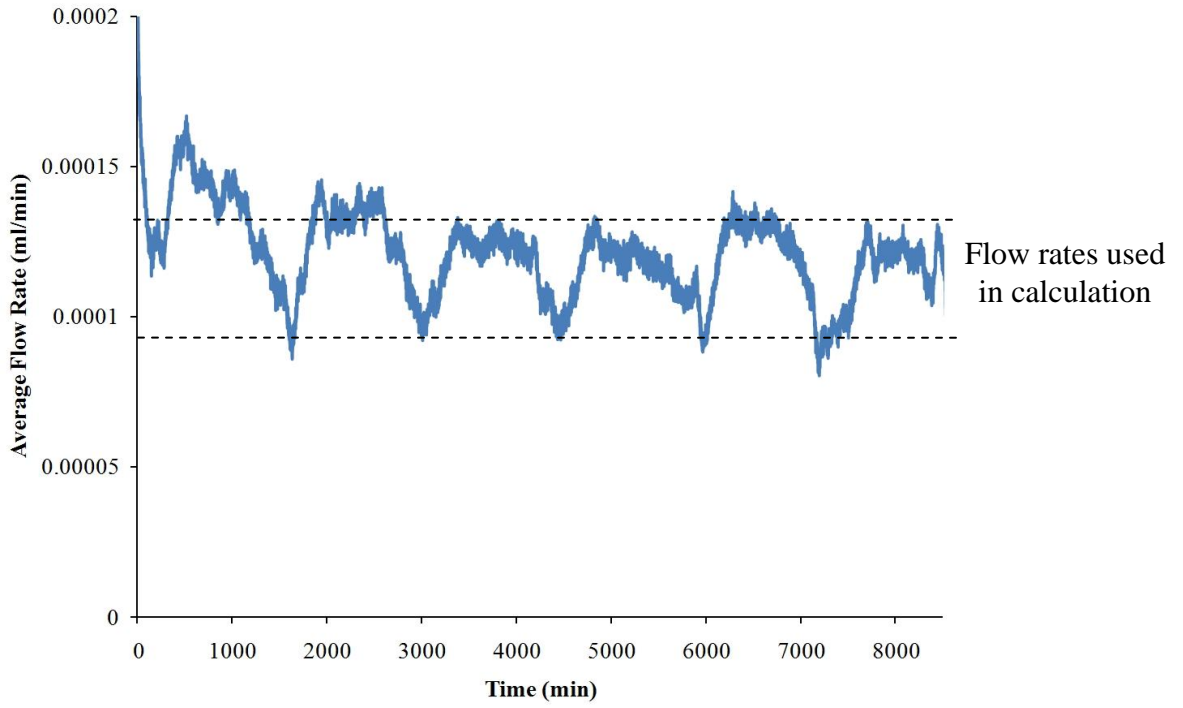
DRG LCL Disk 1 - full surface (dimensions: 75 mm diameter and 4.4 mm thickness)



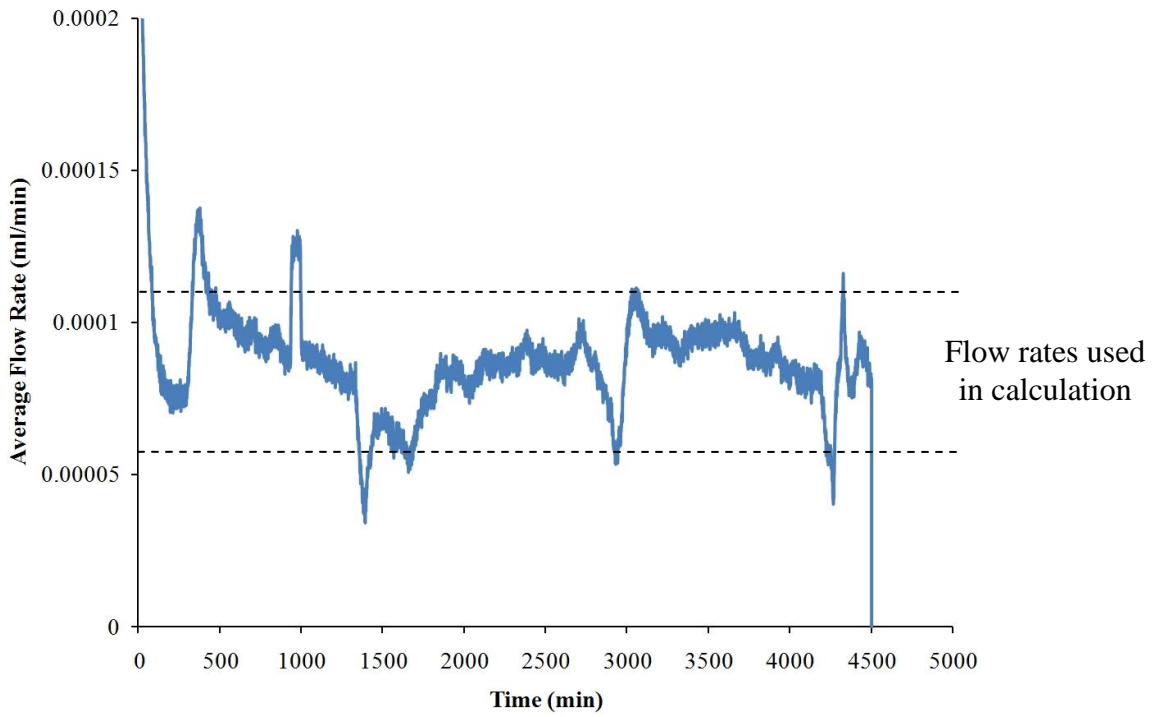
DRG LCL Disk 1 - half surface (dimensions: 75 mm diameter and 4.4 mm thickness)



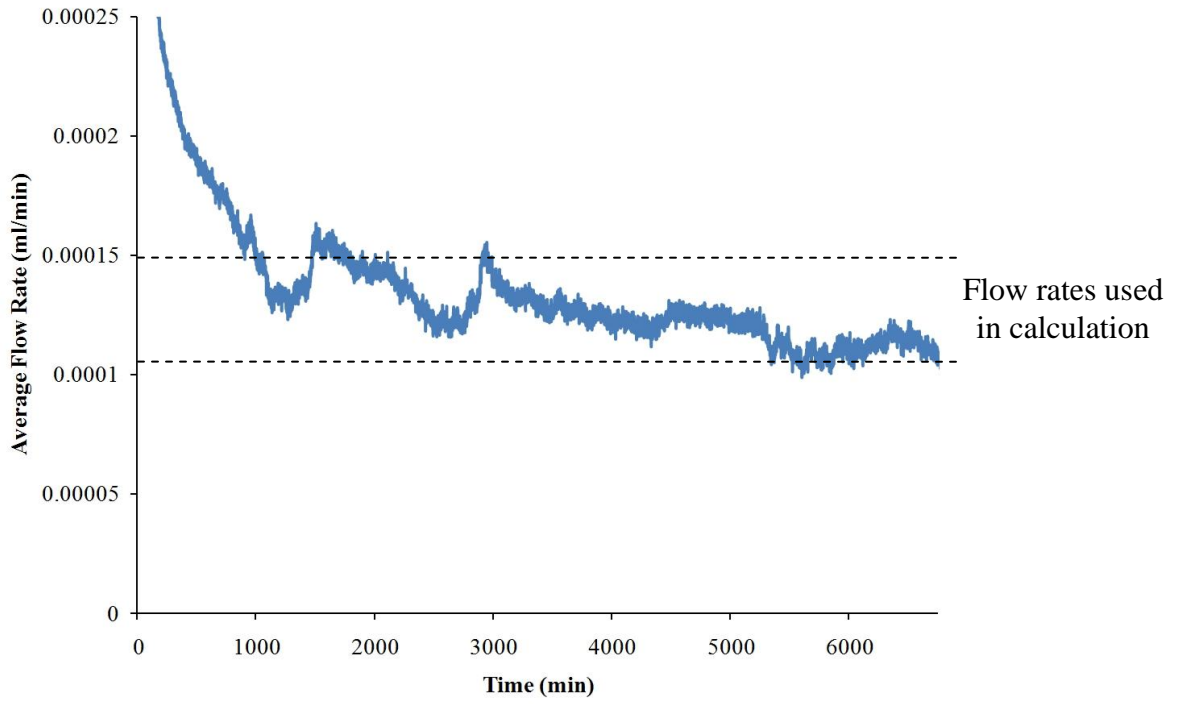
DRG LCL Disk 2 - full surface (dimensions: 75 mm diameter and 5.0 mm thickness)



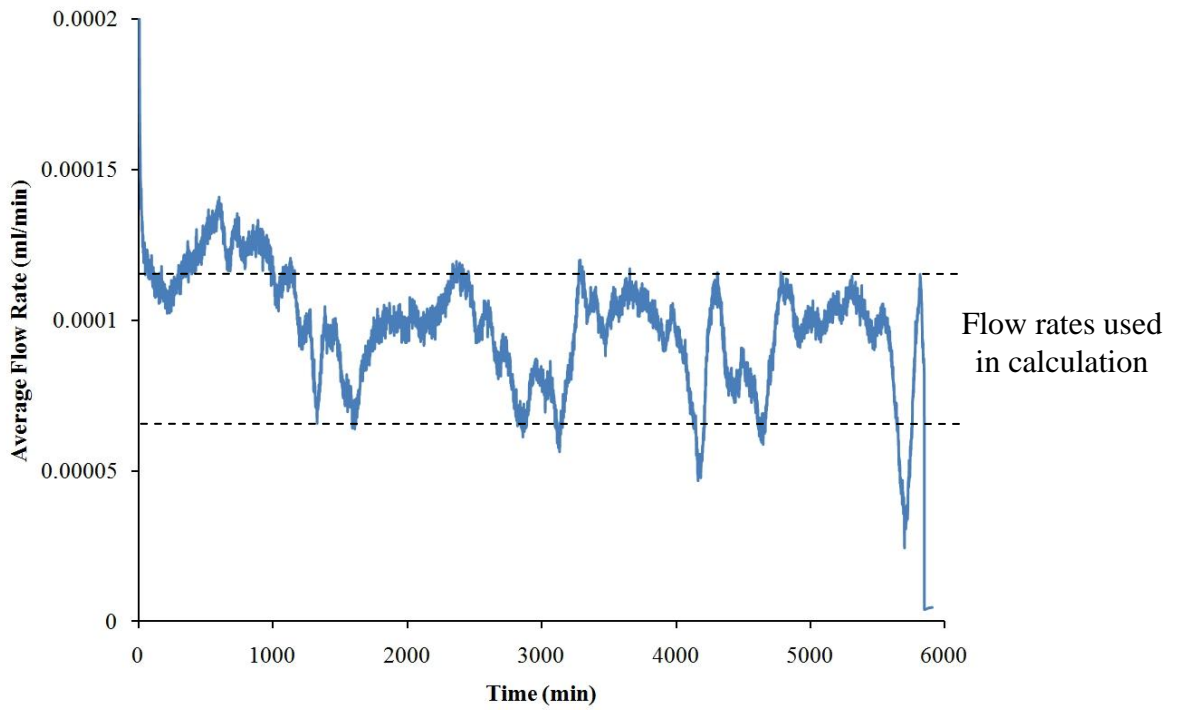
DRG LCL Disk 2 - half surface (dimensions: 75 mm diameter and 5.0 mm thickness)



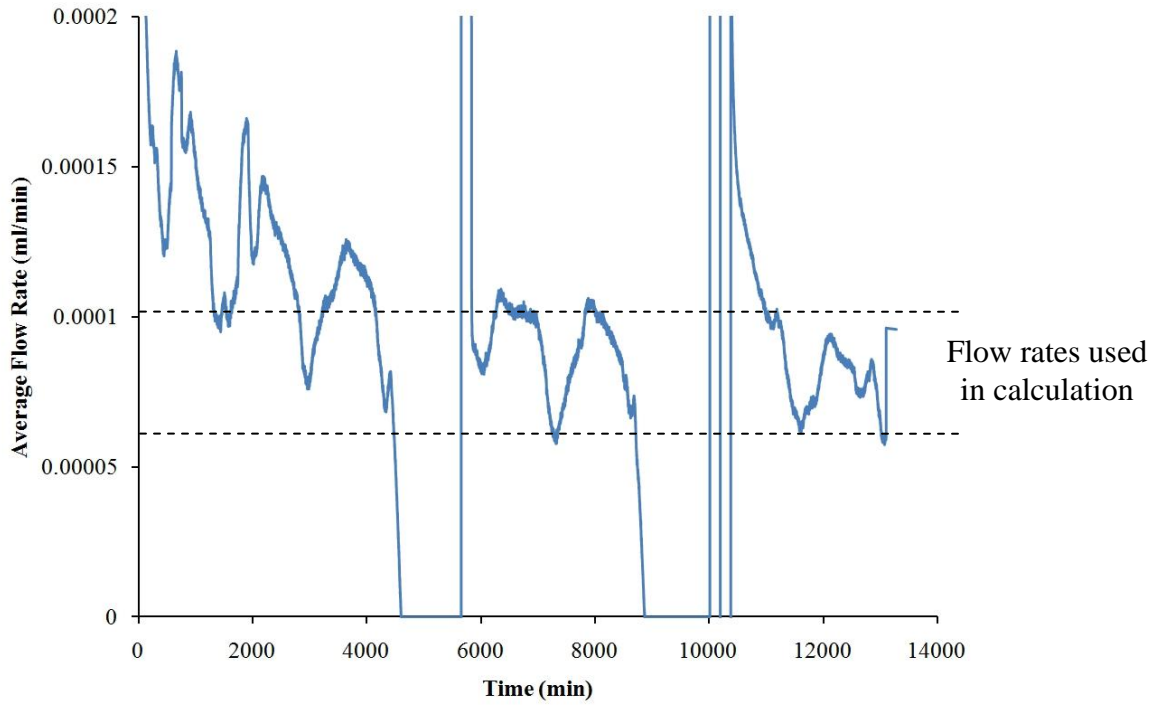
DRG LCL Disk 3 - full surface (dimensions: 75 mm diameter and 4.7 mm thickness)



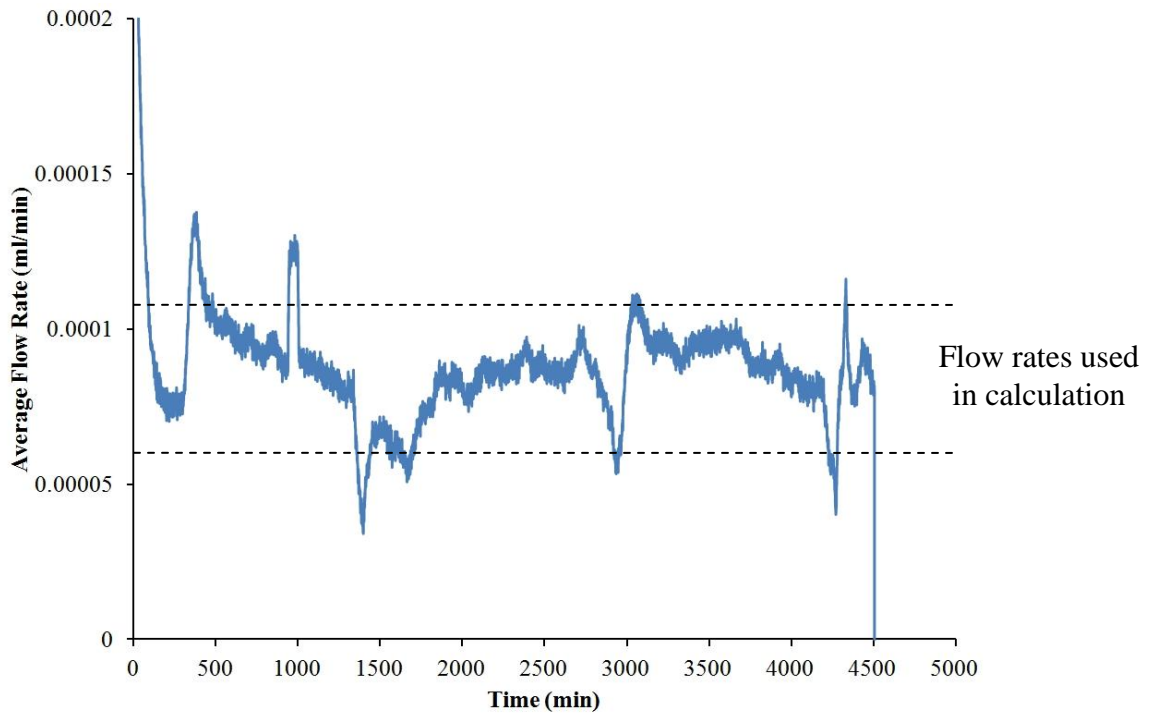
DRG LCL Disk 3 - half surface (dimensions: 75 mm diameter and 4.7 mm thickness)



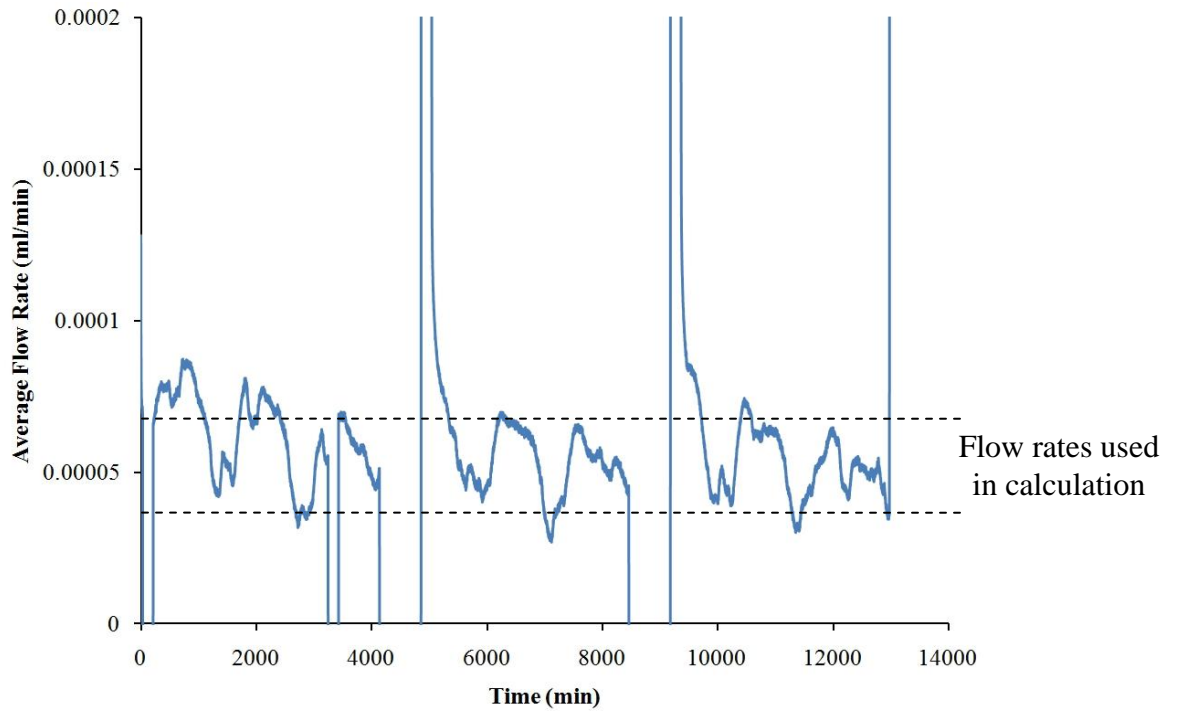
DRG LCL Disk 4 - full surface (dimensions: 75 mm diameter and 5.2 mm thickness)



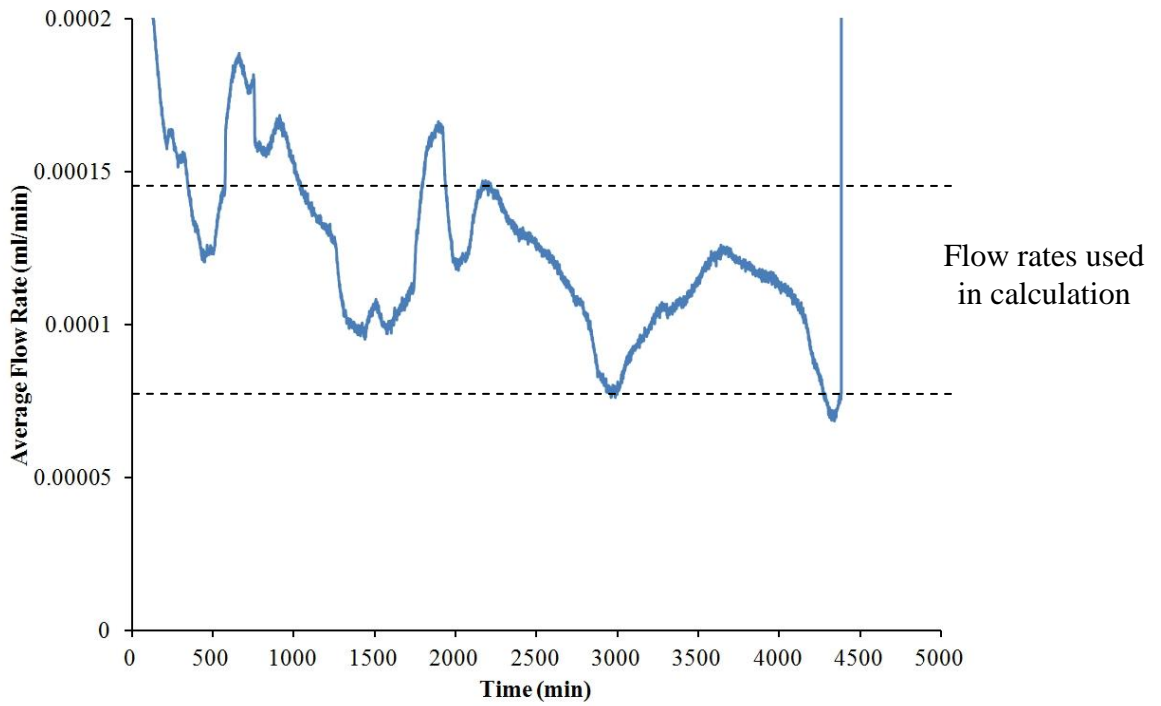
DRG LCL Disk 4 - half surface (dimensions: 75 mm diameter and 5.2 mm thickness)



DRG LCL Disk 5 - full surface (dimensions: 75 mm diameter and 5.0 mm thickness)



DRG LCL Disk 5 - half surface (dimensions: 75 mm diameter and 5.0 mm thickness)



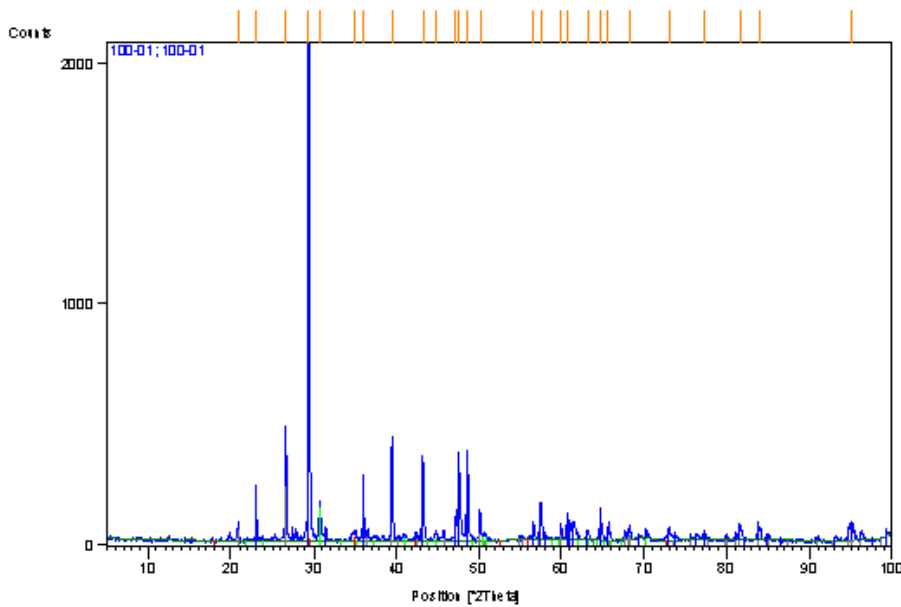
Appendix D: X-ray Diffraction Data

Dark Material (Argillaceous Layers): Luc J 100-01

Anchor Scan Parameters

Dataset Name:	Luc J 100-01
File name:	C:\Program Files\PANalytical\X'Pert Quantify\MR\100-01.XRDML
Sample Identification:	100-01
Measurement Date / Time:	23/06/2010 3:03:14 AM
Operator:	MONIQUE
Raw Data Origin:	XRD measurement (*.XRDML)
Scan Axis:	Gonio
Start Position [°2Th.]:	5.0000
End Position [°2Th.]:	100.0000
Step Size [°2Th.]:	0.0500
Scan Step Time [s]:	1.0000
Scan Type:	Pre-set time
Offset [°2Th.]:	0.0000
Divergence Slit Type:	Automatic
Irradiated Length [mm]:	12.00
Specimen Length [mm]:	10.00
Receiving Slit Size [mm]:	0.3000
Measurement Temperature [°C]:	25.00
Anode Material:	Cu
K-Alpha1 [Å]:	1.54060
K-Alpha2 [Å]:	1.54443
K-Beta [Å]:	1.39225
K-A2 / K-A1 Ratio:	0.50000
Generator Settings:	10 mA, 15 kV
Diffractometer Number:	0
Goniometer Radius [mm]:	200.00
Dist. Focus-Diverg. Slit [mm]:	91.00
Incident Beam Monochromator:	No
Spinning:	Yes

Graphics



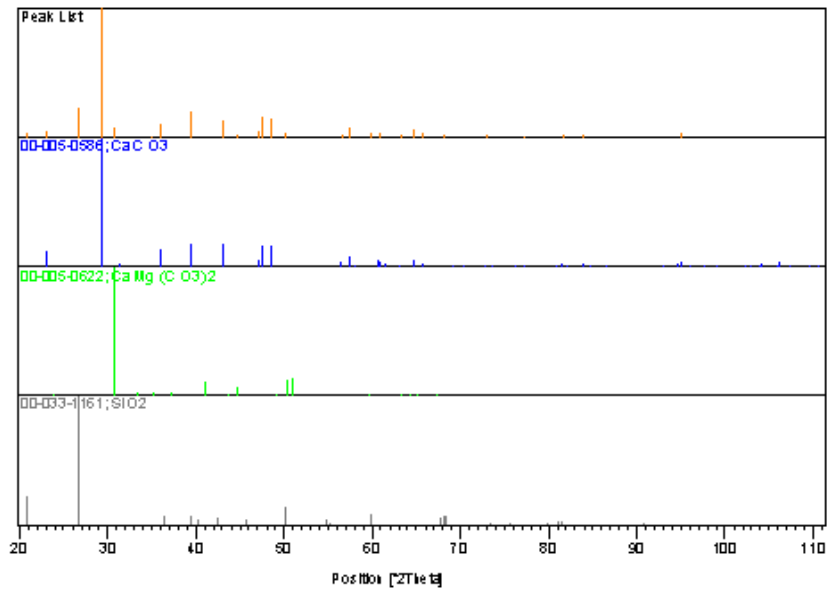
Peak List

Pos. [°2Th.]	Height [cts]	FWHM [°2Th.]	d-spacing [Å]	Rel.Int. [%]	Tipwidth [°2Th.]	Matched by
20.8576	74.74	0.1476	4.25900	3.55	0.1771	00-033-1161
23.0844	97.62	0.1968	3.85296	4.64	0.2362	00-005-0586
26.6400	478.36	0.1476	3.34624	22.74	0.1771	00-033-1161
29.4435	2103.61	0.1476	3.03369	100.00	0.1771	00-005-0586
30.7338	168.58	0.1968	2.90920	8.01	0.2362	00-005-0622
34.9184	32.34	0.5904	2.56956	1.54	0.7085	00-005-0622
36.0215	227.24	0.1968	2.49336	10.80	0.2362	00-005-0586
39.4744	414.76	0.1476	2.28286	19.72	0.1771	00-005-0586
43.2278	295.67	0.1968	2.09295	14.06	0.2362	00-005-0586
44.7570	37.03	0.2952	2.02493	1.76	0.3542	00-005-0622
47.2072	103.15	0.1476	1.92539	4.90	0.1771	00-005-0586
47.5902	347.56	0.1968	1.91078	16.52	0.2362	00-005-0586
48.5994	324.48	0.2460	1.87344	15.42	0.2952	00-005-0586
50.1603	89.32	0.2952	1.81874	4.25	0.3542	00-005-0622
56.6622	52.66	0.2952	1.62451	2.50	0.3542	00-005-0586
57.4897	155.89	0.2460	1.60308	7.41	0.2952	00-005-0586
59.9226	67.56	0.1968	1.54368	3.21	0.2362	00-005-0622
60.8331	87.26	0.3936	1.52274	4.15	0.4723	00-005-0586
63.1996	41.60	0.3936	1.47130	1.98	0.4723	00-005-0586
64.7339	134.86	0.1476	1.44009	6.41	0.1771	00-005-0586
65.6925	78.97	0.1968	1.42138	3.75	0.2362	00-005-0586
68.2330	47.17	0.2952	1.37452	2.24	0.3542	00-033-1161
73.0432	51.97	0.2952	1.29542	2.47	0.3542	00-005-0586
77.3498	34.98	0.2952	1.23370	1.66	0.3542	00-005-0586
81.6214	62.79	0.2952	1.17959	2.98	0.3542	00-005-0586
83.9241	57.09	0.3936	1.15300	2.71	0.4723	00-005-0586
95.0264	74.64	0.7200	1.04457	3.55	0.8640	00-005-0586

Identified components

Visible	Ref.Code	Score	Compound Name	Displ. [°2Th]	Scale Fac.	Chem. Formula
*	00-005-0586	76	Calcite,	0.006	0.948	Ca C O3
*	00-005-0622	35	Dolomite	-0.280	0.069	Ca Mg (C O3)2
*	00-033-1161	36	low quartz, silica	-0.031	0.107	Si O2

Graphics

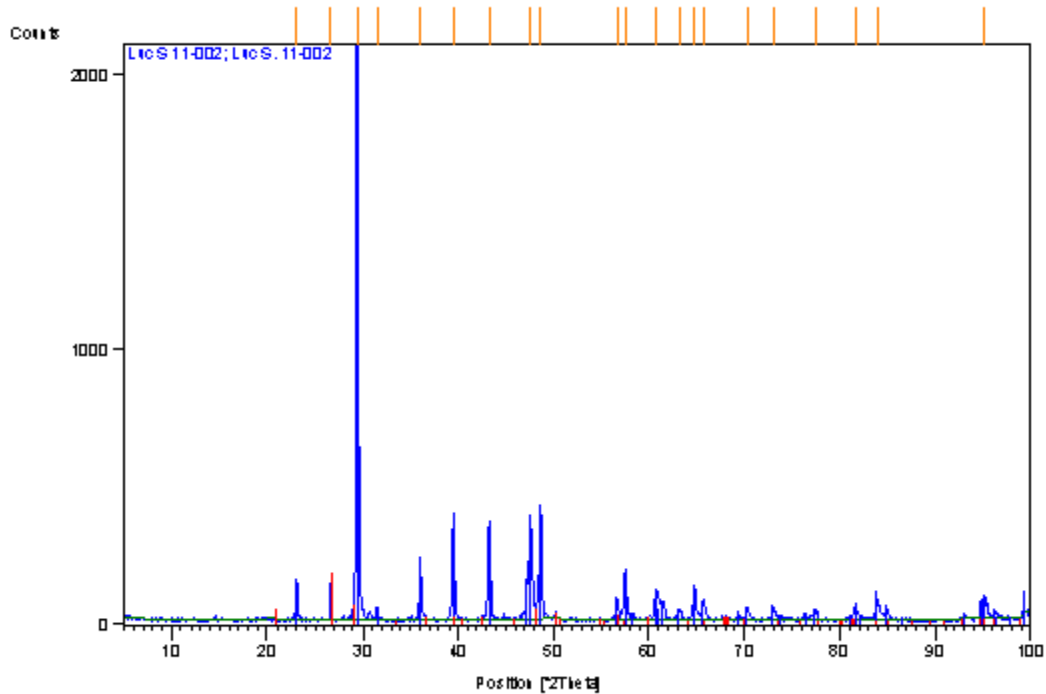


Light Material (Carbonate Layers): Luc S 11-002

Anchor Scan Parameters

Dataset Name:	Luc S 11-002
File name:	C:\Program Files\PANalytical\X'Pert Quantify\MR\Luc S 11-002.XRDML
Sample Identification:	Luc S. 11-002
Measurement Date / Time:	22/06/2010 1:37:42 AM
Operator:	MONIQUE
Raw Data Origin:	XRD measurement (*.XRDML)
Scan Axis:	Gonio
Start Position [°2Th.]:	5.0000
End Position [°2Th.]:	100.0000
Step Size [°2Th.]:	0.0500
Scan Step Time [s]:	1.0000
Scan Type:	Pre-set time
Offset [°2Th.]:	0.0000
Divergence Slit Type:	Automatic
Irradiated Length [mm]:	12.00
Specimen Length [mm]:	10.00
Receiving Slit Size [mm]:	0.3000
Measurement Temperature [°C]:	25.00
Anode Material:	Cu
K-Alpha1 [Å]:	1.54060
K-Alpha2 [Å]:	1.54443
K-Beta [Å]:	1.39225
K-A2 / K-A1 Ratio:	0.50000
Generator Settings:	10 mA, 15 kV
Diffractometer Number:	0
Goniometer Radius [mm]:	200.00
Dist. Focus-Diverg. Slit [mm]:	91.00
Incident Beam Monochromator:	No
Spinning:	Yes

Graphics



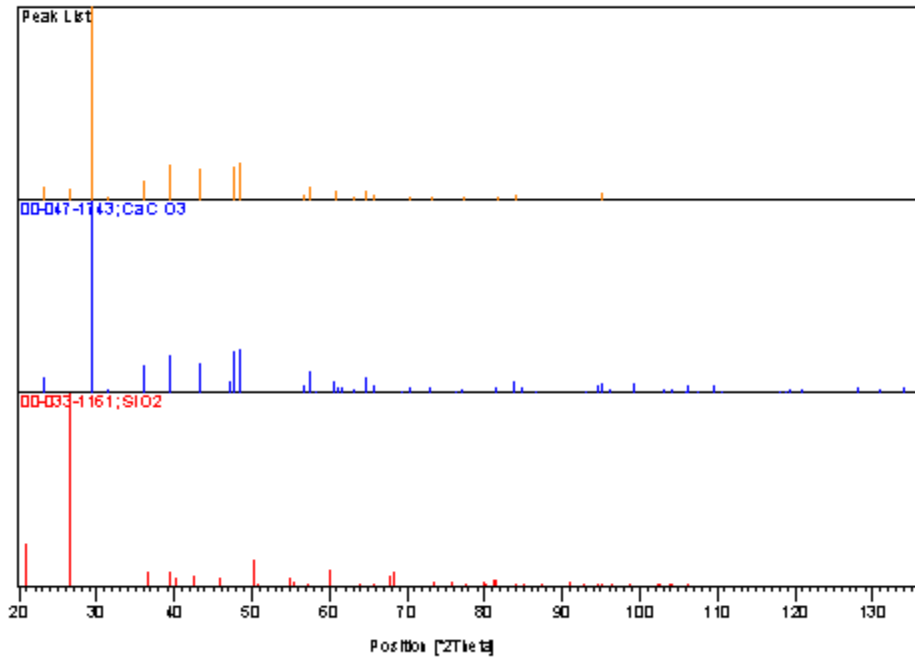
Peak List

Pos.[°2Th.]	Height[cts]	FWHM[°2Th.]	d-spacing[Å]	Rel.Int.[%]	Tipwidth[°2Th.]	Matched by
23.1006	151.44	0.1968	3.85029	7.14	0.2362	00-047-1743
26.6564	137.59	0.1476	3.34421	6.48	0.1771	00-033-1161
29.4670	2122.43	0.1968	3.03132	100.00	0.2362	00-047-1743
31.5229	44.88	0.2952	2.83816	2.11	0.3542	00-047-1743
36.0450	226.86	0.2460	2.49179	10.69	0.2952	00-047-1743
39.4907	394.82	0.1968	2.28196	18.60	0.2362	00-047-1743
43.2492	353.19	0.1968	2.09196	16.64	0.2362	00-047-1743
47.6247	363.83	0.2460	1.90948	17.14	0.2952	00-047-1743
48.6106	416.93	0.2460	1.87303	19.64	0.2952	00-047-1743
56.6954	66.99	0.2952	1.62364	3.16	0.3542	00-047-1743
57.5034	153.86	0.2952	1.60273	7.25	0.3542	00-047-1743
60.8358	104.43	0.3936	1.52268	4.92	0.4723	00-047-1743
63.2114	35.35	0.3936	1.47106	1.67	0.4723	00-047-1743
64.7835	98.97	0.1968	1.43911	4.66	0.2362	00-047-1743
65.7652	64.87	0.3936	1.41999	3.06	0.4723	00-047-1743
70.4017	34.31	0.3936	1.33740	1.62	0.4723	00-047-1743
73.0581	44.30	0.3936	1.29519	2.09	0.4723	00-047-1743
77.3991	37.76	0.3936	1.23303	1.78	0.4723	00-047-1743
81.6445	44.58	0.7872	1.17932	2.10	0.9446	00-047-1743
83.9522	62.52	0.4920	1.15268	2.95	0.5904	00-047-1743
95.1581	77.31	0.8400	1.04347	3.64	1.0080	00-047-1743

Identified components

Visible	Ref.Code	Score	Compound Name	Displ.[°2Th]	Scale Fac.	Chem. Formula
*	00-047-1743	86	Calcite	0.060	0.739	Ca C O3
*	00-033-1161	24	low quartz, silica	0.020	0.082	Si O2

Graphics



Appendix F: Laboratory Equipment

F – 1: Canon EOS Camera

Almost all photographs shown in this thesis (except for the image of the camera itself) were taken with a Canon EOS 500D digital SLR with an EF-S 18-55 IS lens. A tripod was used whenever applicable.



Figure F - 1: Canon EOS 500D camera

F – 2: Circular saw

All cores were cut to a specified length using a circular concrete cutting saw. This tool was manufactured by Target, now a subsidiary of Husqvarna [<http://www.husqvarna.com>] but the blade was obtained through Les Abrasifs Diamantés North Star Ltée [<http://www.northstardia.com>]. This equipment is not a high precision cutter and additional machining was required when dealing with specific requirements for sample length or the need to have parallel faces on a core. The blade is a diamond coated grinding blade that is water cooled. The saw is suitable for cutting hard brittle materials such as concrete or rock but unusable for other materials.



Figure F - 2: Concrete circular saw

F – 3: Cleereman drill press

All the samples used in this research were cored from slabs using this equipment. It is a large drill press with adjustable rpm speed and automatic feed speed. It is an early 20th century machine tool manufactured by Cleereman. Its larger size and rigidity makes it suitable for coring the large slabs to produce cores sufficiently straight to machine to the exact sizes required for these tests.



Figure F - 3: Drill press

F – 4: Coring Equipment

The corers used in the sample retrieval were manufactured by Les Abrasifs Diamantés North Star Ltée [<http://www.northstardia.com>]. Given the variety of samples, several coring bit sizes were required for use. These are diamond coated grinding bits designed to be used with water for cooling and particle removal. The water is fed into the bit through a swivel that forms the attachment piece between the coring bit and the drill press.

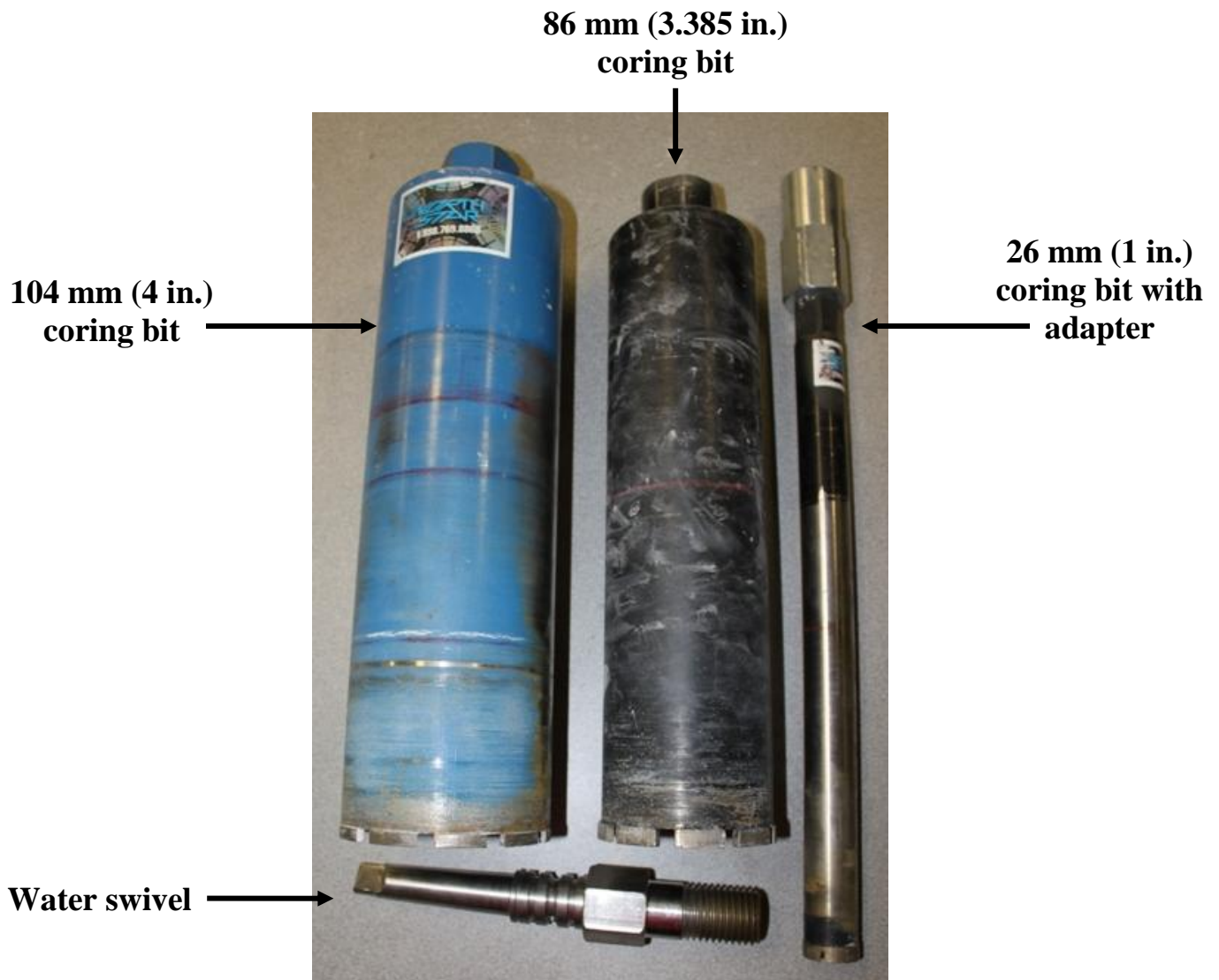


Figure F - 4: Coring tools

Appendix G: Software

MATLAB™

MATLAB™ [<http://www.mathworks.com/index.html>] is a programming environment that is widely used in academic and commercial settings. It is a high level computing language that is more efficient and has greater ease of use than traditional programming languages, such as C, C++ or Fortran. MATLAB provides a visual interface, several program packages for specific applications as well as a large library of free user-made content that is made available through its developer, Mathworks.

ABAQUS™ FEA

ABAQUS™ [<http://www.3ds.com/products/simulia/overview/>] is a finite element based software that is tailored towards engineering applications. It has a practical interface for creating a running model. The software is distributed by Dassault Systems. Version 6,10-EF was used for the modeling done in this thesis.